lubricants

MDPI

Article

Impact of Biosynthesized CeO_2 Nanoparticle Concentration on the Tribological, Rheological, and Thermal Performance of Lubricating Oil

Siraj Azam and Sang-Shin Park *

School of Mechanical Engineering, Yeungnam University, Gyeongsan 38541, Republic of Korea; sirajazam@gmail.com
* Correspondence: pss@ynu.ac.kr

Abstract: This study presents an approach to enhance the performance of lubricating oils through the environmentally friendly synthesis of cerium oxide (CeO_2) nanoparticles using Moringa oleifera leaf extract. These biosynthesized nanoparticles were thoroughly characterized for their structural and thermal stability by utilizing X-ray diffraction, scanning electron microscopy, and transmission electron microscopy. The CeO_2 nanolubricants, prepared at various concentrations, displayed significant improvements in viscosity, stability, and thermal conductivity. Specifically, the 0.15 wt% concentration achieved the best performance, reducing viscosity to 9.79 pascal-second (Pa·s) at 80 °C while exhibiting excellent dispersion and minimal sedimentation over time. The thermal conductivity tests revealed a notable 43% increase in heat transfer efficiency at higher nanoparticle concentrations. Tribological tests conducted using a tribometer demonstrated significant improvements in the lubrication properties. The nanolubricant with a 0.15 wt% concentration of CeO_2 nanoparticles achieved the lowest friction coefficient, showing an approximate 26% reduction compared to the base oil, along with a notable decrease in wear rate. This study demonstrates the potential of biosynthesized CeO_2 nanoparticles as effective, sustainable additives in lubricating oils, providing improved thermal, rheological, and tribological properties and marking a significant step toward eco-friendly lubrication solutions.

Keywords: cerium oxide; biosynthesis; nanolubricants; tribology; thermal conductivity; rheology

Citation: Azam, S.; Park, S.-S. Impact of Biosynthesized CeO_2 Nanoparticle Concentration on the Tribological, Rheological, and Thermal Performance of Lubricating Oil. *Lubricants* **2024**, *12*, 400. https://doi.org/10.3390/lubricants12110400

Received: 23 September 2024
Revised: 13 November 2024
Accepted: 19 November 2024
Published: 20 November 2024

1. Introduction

In recent years, the use of nanoparticles in lubricants has revolutionized the field of tribology, offering a path to significantly enhance lubrication performance by improving properties such as friction reduction, wear resistance, and thermal stability. Lubricating oils play an essential role in reducing mechanical friction, wear, and energy consumption in a wide range of machinery across industries like automotive, manufacturing, aerospace, and energy. As the demand for machinery has increased, traditional lubricants have struggled to meet the higher performance expectations. Consequently, researchers have focused on developing advanced lubricant formulations incorporating nanoparticles to address these limitations. Nanoparticles exhibit unique properties due to their high surface area, chemical reactivity, and size-dependent physical characteristics. These attributes make them highly effective in improving the lubricant performance by modifying surface interactions between moving parts and enabling better thermal management. A variety of nanoparticles have been investigated as lubricant additives including zinc oxide (ZnO), copper oxide (CuO), titanium dioxide (TiO_2), molybdenum disulfide (MoS_2), and silicon dioxide (SiO_2), among others. Each type of nanoparticle offers specific benefits, such as improving anti-wear performance, reducing friction, or enhancing heat dissipation, making them promising candidates for the development of high-performance lubricants. The common nanoparticle properties and their functions in the lubricants are listed in Table 1.

Table 1. Common nanoparticles used in lubricants and their properties.

S. No.	Nanoparticle	Properties	Function in Lubricants	References
1.	Zinc Oxide (ZnO)	High hardness, thermal stability, chemically stable	Anti-wear, reduces friction under extreme pressure	[1–3]
2.	Copper Oxide (CuO)	High thermal conductivity, small size, high surface energy	Enhances thermal conductivity, reduces wear and friction	[4,5]
3.	Titanium Dioxide (TiO_2)	High hardness, excellent thermal stability, photocatalytic properties	Reduces friction and wear, enhances thermal conductivity	[6–8]
4.	Molybdenum Disulfide (MoS_2)	Layered structure, chemically stable, low friction coefficient, high thermal stability	Reduces friction and wear, effective in high-temperature applications	[9,10]
5.	Silicon Dioxide (SiO_2)	Thermal stability, low chemical reactivity, high hardness	Forms protective film, reduces friction, improves thermal stability	[11,12]
6.	Graphene	High mechanical strength, excellent thermal conductivity, low friction	Solid lubricant, reduces friction, improves load-bearing capacity	[13,14]
7.	Tungsten Disulfide (WS_2)	Layered structure, high pressure tolerance, low friction coefficient	Solid lubricant, reduces friction and wear under high-pressure conditions	[15,16]

Among the nanoparticles explored, cerium oxide (CeO_2) nanoparticles are particularly notable for their unique redox properties [17] and ability to form self-healing tribofilms [18] on lubricated surfaces. CeO_2 nanoparticles are unique in that they can switch between Ce^{3+} and Ce^{4+} oxidation states [19,20], which enable them to repair damaged surfaces by forming protective layers under frictional stress. Studies indicate that this adaptive tribofilm formation helps to repair minor surface damage, enhancing surface stability by creating a resilient protective layer [21]. Additionally, CeO_2 nanoparticles exhibit a high surface area and catalytic activity [22,23], which facilitate a better interaction with the lubricating oil, reducing friction and wear at the nanoscale. This combination of redox-driven tribofilm formation and surface area benefits makes CeO_2 highly effective in improving the tribological and thermal performance of lubricants. The tribological outcomes from both assessments illustrate that CeO_2 nanoparticles exhibit qualities conducive to reducing friction and providing extreme pressure performance [24]. These properties contribute to their ability to reduce friction and wear in tribological applications, which is critical in industries where machinery must operate under extreme pressure and temperatures [25]. The inclusion of CeO_2 nanoparticles in lubricants is part of a broader trend toward using nanotechnology to enhance the performance and sustainability of industrial lubricants. As industries seek to minimize their environmental impact, there is a growing demand for lubricants that not only improve the machinery performance, but also reduce energy consumption and emissions. This has spurred the development of eco-friendly nanolubricants that leverage the unique properties of nanoparticles to reduce friction, wear, and energy losses in mechanical systems. Moreover, by enhancing the thermal conductivity of lubricants, nanoparticles like CeO_2 can improve heat dissipation in machinery, preventing overheating and reducing the risk of mechanical failure.

Traditional synthesis techniques for CeO_2 nanoparticles typically involve the use of chemical precursors and high-temperature processes [26]. In these methods, cerium salts or compounds are subjected to high temperatures [27–29], resulting in the formation of CeO_2 nanoparticles. While effective, these conventional techniques have certain drawbacks: they often require the use of hazardous chemicals [30] and high energy input, leading to a substantial environmental footprint. Additionally, the by-products and waste generated during these processes can contribute to pollution and environmental degradation [31]. On the other hand, biosynthesis methods of nanoparticles offer a more environmentally friendly alternative [32–34]. These techniques harness the power of biological organisms or natural materials to facilitate the reduction and stabilization of cerium ions into nanoparticles. One previous study [35] discussed the challenges of achieving precise and efficient in vivo drug delivery using magnetic micro-/nanorobots. The proposed solution involves a novel strategy using magnetic biohybrid microrobot multimers (BMMs) based on Chlorella cells. Another study [36] utilized the aqueous seed extract of Nigella sativa for the green synthesis of zero-valent iron nanoparticles (ZVI-NPs), demonstrating efficient heavy metal remediation in industrial wastewater. Characterized by various techniques, cylindrical ZVI-NPs

with surface functional groups showed high removal efficiency, biological compatibility, and potential anticancer properties, indicating their promising application for eco-friendly heavy metal remediation. Such processes typically occur under mild conditions, reducing the need for high temperatures and harsh chemicals [37]. As a result, biosynthesized CeO_2 nanoparticles tend to have a lower inherent toxicity as well as a reduced environmental impact compared to those produced through traditional chemical routes. The environmental benefits associated with the use of biosynthesized CeO_2 nanoparticles stem from several scientifically grounded factors. First, the process of biosynthesis often involves the use of natural sources or microorganisms to produce these nanoparticles. The resulting CeO_2 nanoparticles tend to have a lower level of inherent toxicity due to their biogenic production, making them less harmful to ecosystems and living organisms when they eventually enter the environment [38]. What distinguishes this study is its pioneering approach to producing CeO_2 nanoparticles using biosynthesis, which sets it apart from traditional production methods known for their resource-intensive and environmentally detrimental processes. Biosynthesis harnesses the capabilities of biological organisms to generate nanoparticles, presenting a sustainable alternative that not only addresses concerns related to the ecological impact of nanomaterials, but also aligns seamlessly with the global drive toward environmentally conscious practices. The study, conducted on the incorporation of biosynthesized CeO_2 nanoparticles as additives in PAO oil, represents a comprehensive exploration into the realm of lubrication science and materials engineering.

The primary objective of this research was to assess the effectiveness of biosynthesized CeO_2 nanoparticles as additives in PAO oil, focusing on improvements in friction, wear, and thermal conductivity. These CeO_2 nanoparticles, produced through environmentally friendly methods, help to minimize the environmental impact of the production process. The tribological performance of the CeO_2 nanolubricants was evaluated using a reciprocating tribometer, which measures friction and wear under controlled conditions, providing data on the coefficient of friction and specific wear rates. This study also investigated the thermal conductivity of PAO oil enhanced with CeO_2 nanoparticles, a critical factor for high-temperature machinery. Efficient heat dissipation prevents overheating and ensures both lubricant and machinery longevity. The high thermal stability of CeO_2 nanoparticles makes them particularly suitable for improving the thermal management of lubricants. Additionally, this research explored the rheological properties of the CeO_2-infused oil, which affect the lubricant's flow behavior under various temperature and pressure conditions. Nanoparticles can alter the viscosity and flow characteristics, influencing the oil's ability to provide effective lubrication. By examining these properties, we aimed to understand how CeO_2 nanoparticles impact the overall performance of PAO oil. This research contributes to the growing knowledge on the use of biosynthesized nanoparticles in lubricants, offering both performance enhancements and more sustainable manufacturing practices. The findings have implications for industries looking to improve efficiency while reducing their environmental footprint, highlighting the potential of CeO_2 nanoparticles as valuable additives for next-generation lubricants.

2. Materials and Methods

2.1. Synthesis of CeO_2 Nanoparticles

The synthesis of CeO_2 nanoparticles, as illustrated in Figure 1, was adapted from a previous study [39]. Fresh leaves of Moringa oleifera were selected and sterilized by immersing them in a 1% sodium hypochlorite solution for 10–15 min, followed by thorough rinsing with double-distilled water (DDW). The sterilized leaves were then dried in the shade for 2–3 days. Once dried, the leaves were ground into a fine powder using a mixer grinder. To obtain the methanolic extract, 25 mg of the powdered leaves were mixed with 200 mL of methanol and left for 24 h. The resulting solution was filtered using Whatman filter paper No. 1. For the synthesis, 1.86 g of cerium nitrate salt with high purity chemicals was purchased from Sigma Aldrich and used without further purification. This was dissolved in 50 mL of distilled water and stirred magnetically at 65 °C. Gradually,

25 mL of the methanolic leaf extract was added dropwise to the cerium nitrate solution. As the solution mixed, its color changed from dark brown to light brown, signaling the progress of the reaction. The reaction was halted once the solution developed a sticky consistency. The mixture was collected in a Petri dish and oven-dried at 80 °C. Afterward, it was heated in a furnace at 400 °C. The dried material was finely ground using a mortar and pestle, resulting in the formation of a yellow CeO_2 nanoparticle powder that was subsequently used for characterization.

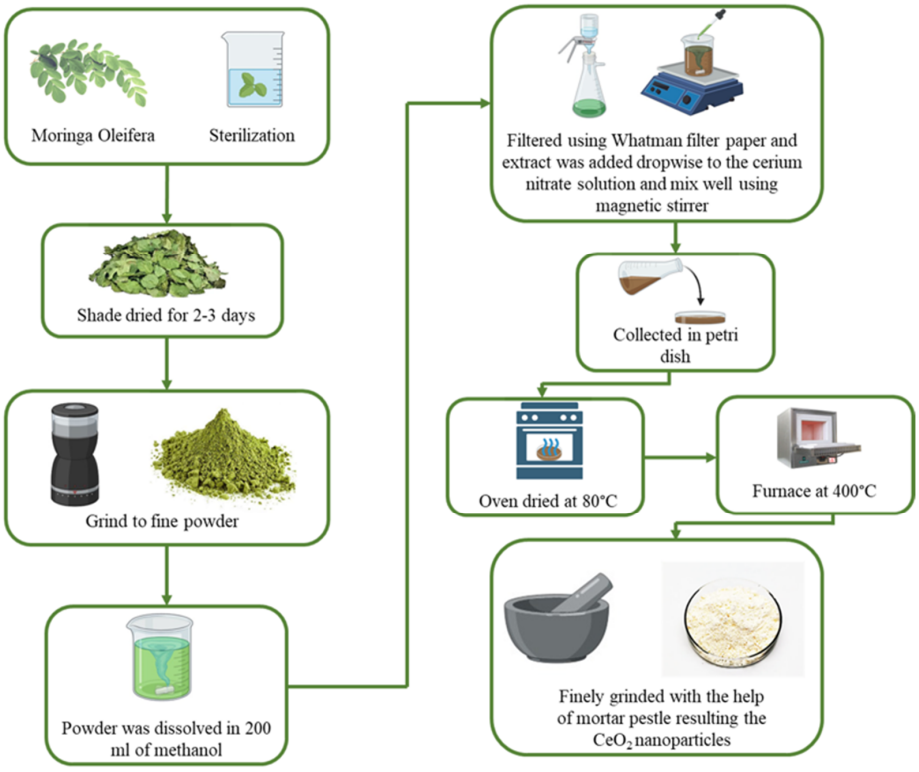

Figure 1. Biosynthesis process of CeO_2 nanoparticles.

2.2. Structural Characterization

For the structural characterization of the CeO_2 nanoparticles, a Panalytical (Almelo, The Netherlands, XPERT PRO) X-ray diffractometer was employed using Cu-Kα radiation (λ = 1.5406 Å) and operating within a 2θ range of 20 to 80°. This XRD technique is highly effective in revealing the crystalline properties of CeO_2 nanoparticles including crystal size, lattice parameters, and phase composition [22,40,41]. In addition, high-resolution imaging was achieved using a UHR-FESEM (ultrahigh resolution field emission scanning electron microscope) Hitachi (Tokyo, Japna) SU-8600, which provided detailed insights into the surface morphology and structural features [40]. For even more in-depth analysis, a TEM (transmission electron microscopy) Hitachi H-7600 at 120 kV was utilized to closely examine individual nanoparticles, further elucidating their nanoscale characteristics [42]. All the instruments are sourced from Central Equipment Center (Yeungnam University, Gyeongsan, Republic of Korea).

2.3. FTIR

Fourier transform infrared (FTIR) spectroscopy was performed to identify the molecular fingerprint of the synthesized CeO_2 nanoparticles using a Perkin-Elmer (Waltham, MA, USA, Spectrum 100) FTIR instrument sourced from Central Equipment Center (Yeungnam University, Gyeongsan, Republic of Korea). This technique involves exposing the nanoparticles to infrared radiation, allowing the instrument to detect the vibrational modes within the material [43,44]. The high precision and sensitivity of the Perkin-Elmer Spectrum 100 FTIR make it an excellent tool for capturing the absorbed emissions from the

nanoparticles, offering valuable insights into their chemical composition and confirming the purity of the synthesized samples. These findings are essential for understanding the chemical characteristics and ensuring the high quality of CeO_2 nanoparticles, supporting their potential applications in nanotechnology.

2.4. TGA

Thermogravimetric analysis (TGA) was conducted to examine the thermal behavior of the synthesized CeO_2 nanoparticles using a TA Instruments (New Castle, DE, USA, SDT Q600) sourced from Central Equipment Center (Yeungnam University, Gyeongsan, Republic of Korea). This instrument is designed for precise analysis of thermal stability. TGA was performed at a heating rate of 10 °C/min in a nitrogen-controlled environment, allowing for the accurate tracking of mass changes relative to temperature. This approach provides detailed insights into the material's thermal decomposition [45,46]. The analysis was carried out over a temperature range of 25 °C to 800 °C, enabling a comprehensive assessment of the thermal stability profile of the CeO_2 nanoparticles, which is essential for understanding their performance under varying thermal conditions.

2.5. Rheological Properties

This study investigated the rheological properties of both pure oil and a range of nanolubricants at temperatures of 40, 60, 80, and 100 °C. The Anton Paar (Graz, Austria, MCR 302e) sourced from Central Equipment Center (Yeungnam University, Gyeongsan, Republic of Korea), an advanced instrument designed for rheological analysis, played a pivotal role in this examination. The measurements were carried out using a plate–plate setup with a 0.3 mm gap, testing all concentrations of the nanolubricants. This thorough approach provides a detailed understanding of how these fluids react to temperature variations, shear rates, and the complex interactions between these factors. The Anton Paar (MCR 302e) excels in analyzing the changes in viscosity of both pure oil and nanolubricants across different temperatures, aiding in the optimization of lubrication strategies for diverse operational environments.

2.6. Thermal Conductivity

The thermal conductivity of both pure oil (PO) and various nanolubricants was assessed to better understand their thermal properties by using the TEMPOS thermal properties analyzer by Meter Group (Pullman, WA, USA) sourced from Energy Management and Storage Laboratory (Yeungnam University, Gyeongsan, Republic of Korea). TEMPOS provides a precise method for evaluating the heat transfer characteristics of lubricants. To ensure the accuracy of the measurements, the instrument was first calibrated with a glycerin sample of known standard thermal conductivity. Once validated, tests on the prepared samples were conducted in "unattended mode", allowing the device to automatically take multiple readings at set intervals, ensuring reliable data collection. The analysis was performed at an ambient temperature, enabling a comprehensive assessment of the thermal behavior of the lubricants. The collected data, represented as average values, were plotted for detailed analysis. This systematic approach, combined with the advanced functionality of TEMPOS, highlighted subtle differences in thermal conductivity between pure oil and the nanolubricants, providing a strong foundation for optimizing lubrication strategies across various applications.

2.7. Preparation of Nanolubricants

The nanolubricants were prepared by dispersing varying amounts of CeO_2 nanoparticles into PAO oil at concentrations of 0.05, 0.1, 0.15, and 0.2 wt%, as shown in Figure 2. Each mixture was initially placed in an ultrasonication bath for 1 h to promote proper dispersion of the nanoparticles. Following ultrasonication, the mixtures were subjected to vortex mixing for 15 min to ensure a uniform distribution of the nanoparticles throughout the oil. To assess the stability of the prepared nanolubricants, the samples were allowed to stand for 15 days. Figure 2 (Day 15) demonstrates the dispersion stability of the nanolubricants, with only minor sedimentation observed, indicating that the nanolubricants remained relatively well-dispersed over time.

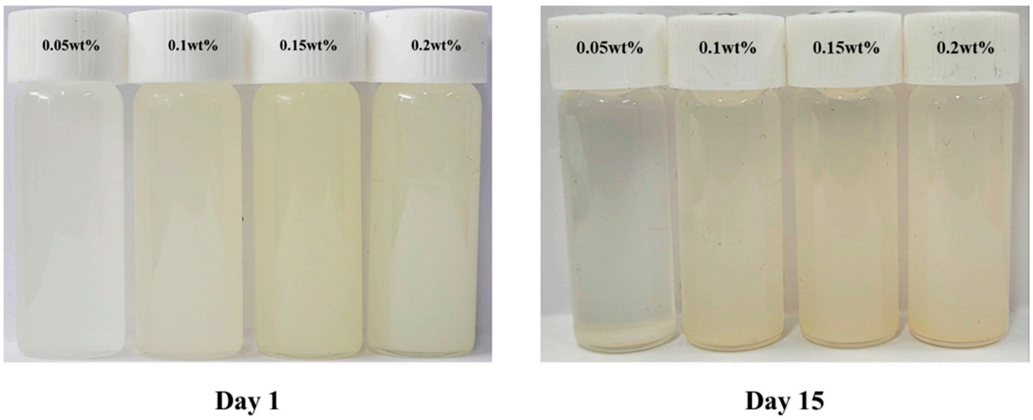

Figure 2. Nanolubricants prepared on day 1 and after 15 days, demonstrating stability over time.

2.8. Experimental Setup for Tribology Test

The reciprocating tribometer used in this study was specifically designed for precise tribological testing, allowing for a wide range of test configurations. It features a fixed motor that provides vertical motion to the pin under controlled loads, while its detachable components offer flexibility for various setups including pin-on-disc, reciprocating, and rotating shaft tests. This adaptability allows the tribometer to be tailored to specific testing needs, ensuring accurate and reliable results. Operating the tribometer is straightforward, with a touchscreen control panel and specialized software that enables precise adjustments of parameters such as load, frequency, stroke length, and test distance. Test data are automatically saved in Excel format for easy transfer and detailed analysis. In this study, the tribometer was used in the reciprocating configuration, where the pin moves vertically under the applied load, and the plate moves horizontally to simulate real-world reciprocating motion. To ensure the homogeneity of the prepared samples, 10 min of ultrasonication followed by 5 min of vortex mixing was used immediately before testing. The pin and sliding plate were made of heat-treated AISI 1045 steel with a hardness of 210 HB (Brinell hardness) and a surface roughness (Ra) of 0.9 µm. The testing parameters included a 10 N load, 3 Hz frequency, 25 mm stroke length, and a total running distance of 840 m, using a steel-to-steel contact setup, as illustrated in Figure 3.

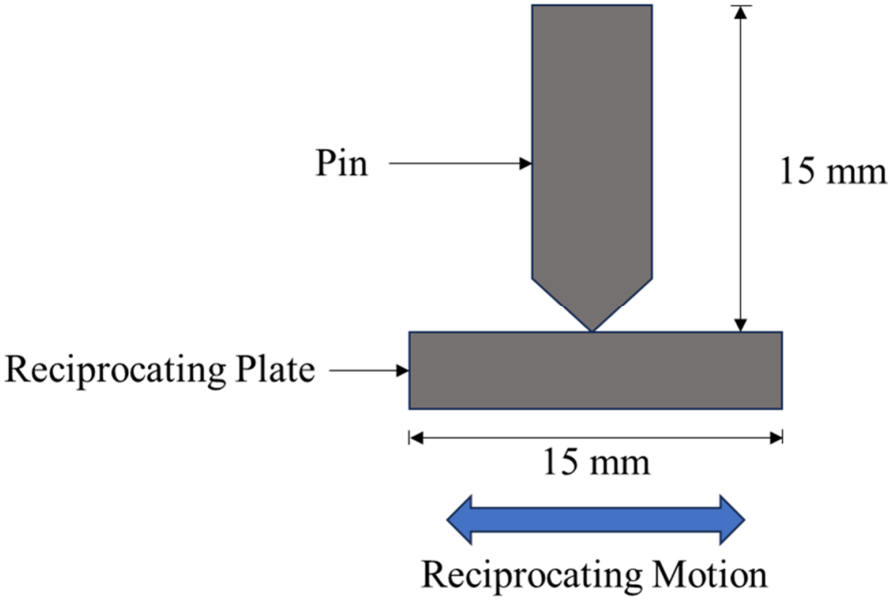

Figure 3. Schematics of the testing pin and reciprocating plate.

3. Results

3.1. XRD Diffraction

Figure 4 presents the XRD pattern of the synthesized CeO_2 nanoparticles, revealing their crystalline structure. Prominent peaks were observed at 2θ angles of 28.40°, 33.08°, and 47.45°, which corresponded to the (111), (200), and (220) crystallographic planes of CeO_2, respectively. These peaks indicate the high crystallinity of the sample and align with the expected reflections for the face-centered cubic (fcc) phase structure of CeO_2, as referenced by JCPDS data card no. 34-0394 [47]. Additional diffraction peaks at 2θ values of 56.30°, 59.17°, 69.38°, 76.77°, and 79.00°, corresponding to the (311), (222), (400), (331), and (420) planes, further confirmed the complete crystallographic profile of the nanoparticles. The presence of these well-defined peaks affirmed the structural integrity and uniformity of the CeO_2 nanoparticles. Importantly, the absence of extraneous peaks confirmed the high phase purity of the synthesized material, indicating that no secondary phases or impurities were present. This XRD analysis elucidates the well-ordered crystalline structure of CeO_2 nanoparticles, validating both their structural integrity and purity. The data affirm the suitability of these nanoparticles for potential applications in nanotechnology and materials science.

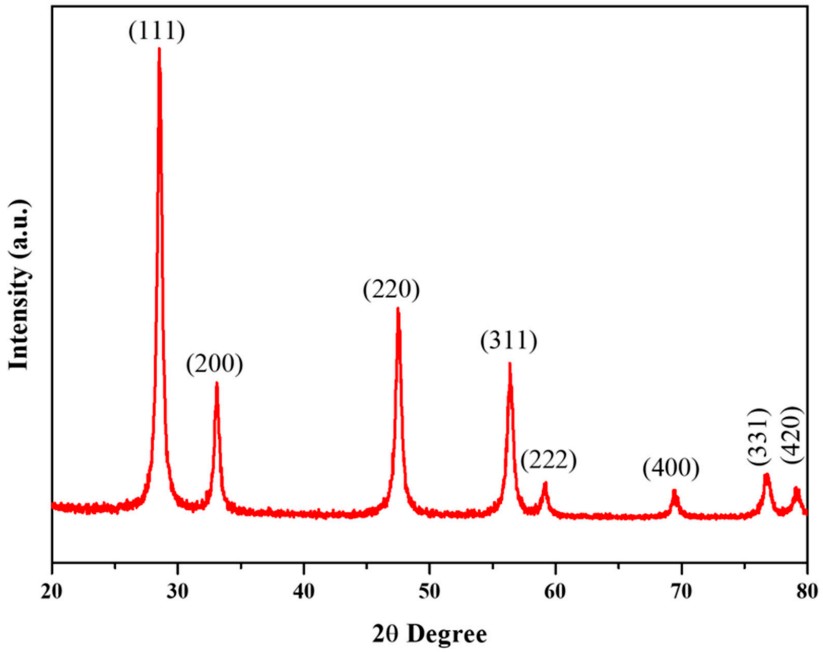

Figure 4. XRD diffraction peaks of CeO_2.

3.2. Morphological Characterization

The morphological characterization of the CeO_2 nanoparticles synthesized in this study was carried out using SEM, EDX, and TEM analyses. These characterization techniques provide critical insights into the structure, size, and elemental composition of the nanoparticles. The SEM images in Figure 5 reveal the surface morphology and apparent size distribution of the CeO_2 nanoparticles at different magnifications. In Figure 5a, at the 1 µm scale, the particles appeared irregularly shaped and agglomerated, a common characteristic for nanoparticles synthesized via biosynthesis due to their high surface energy, which promotes clustering. At the 500 nm scale in Figure 5b, the individual particles were more distinguishable within the agglomerates. Figure 5c provides a closer view at a 200 nm scale, showing that the agglomerates were approximately 200 nm in size. It is important to note that SEM captures surface features and may represent aggregated particle clusters rather than individual nanoparticle sizes. Additionally, SEM samples typically require a thin conductive coating (such as gold or carbon) to prevent charging effects, which may slightly increase the apparent size of the particles due to the coating layer. The rough

surfaces and stacked arrangement observed in the SEM images indicate a high surface area. The energy-dispersive X-ray spectroscopy (EDX) spectrum in Figure 6 was acquired from SEM mapping to confirm the elemental composition of the CeO_2 nanoparticles. The EDX spectrum showed prominent peaks corresponding to cerium (Ce) and oxygen (O), which are the primary constituents of CeO_2. The quantitative analysis revealed that Ce constituted approximately 81.81% by weight, while oxygen made up 18.19%, aligning well with the stoichiometric composition expected for CeO_2. Less significant peaks for impurities or other elements were detected, confirming the high purity of the synthesized nanoparticles. The EDX mapping of the surface indicates a uniform distribution of cerium and oxygen across the nanoparticles, further supporting the successful synthesis of CeO_2 nanoparticles with minimal contamination.

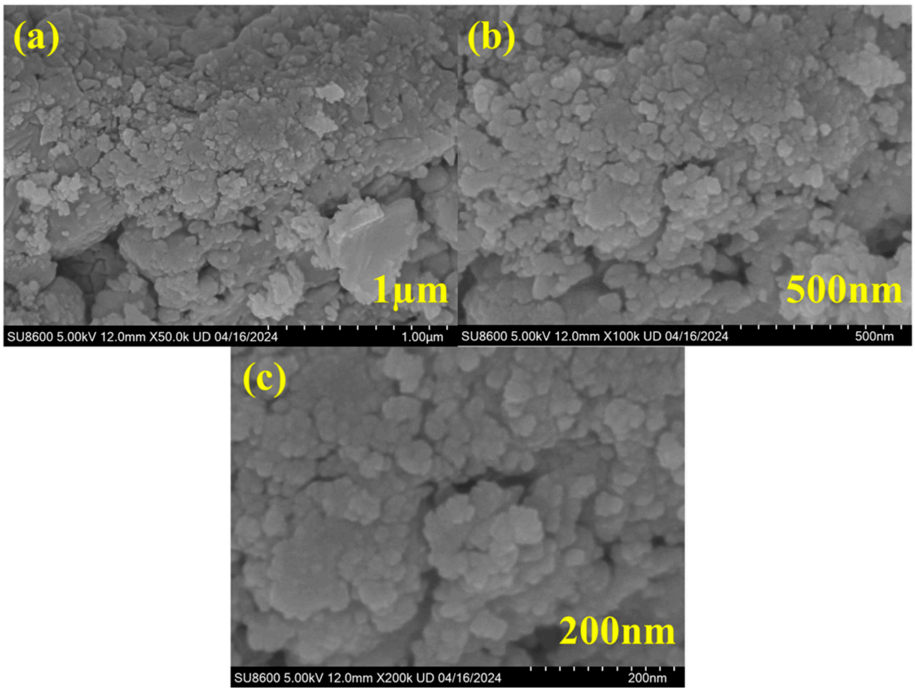

Figure 5. SEM images of the CeO_2 nanoparticles at the (**a**) 1 µm, (**b**) 500 nm, and (**c**) 200 nm scale.

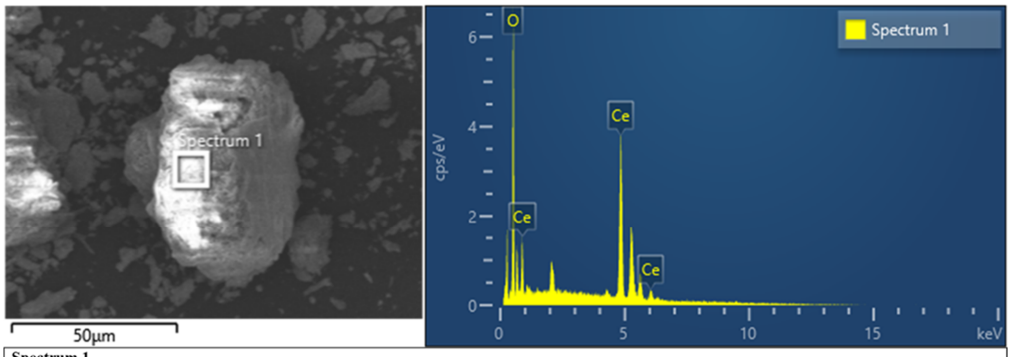

Spectrum 1

Element	Signal Type	Line	Wt%	Wt% Sigma	Atomic %
O	EDS	K series	18.19	0.36	66.07
Ce	EDS	L series	81.81	0.36	33.93
Total			100.00		100.00

Figure 6. EDX taken from the SEM mapping of CeO_2 nanoparticles.

Transmission electron microscopy (TEM) was employed to examine the finer details of the CeO_2 nanoparticles, providing high-resolution images of their internal structure, as shown in Figure 7. In Figure 7a, a low-magnification image at the 200 nm scale showed that the CeO_2 nanoparticles tended to form clusters due to their high surface energy. However,

Figure 7b, at the 50 nm scale, revealed the individual particle size within these clusters, with particles ranging from 25 to 70 nm in diameter. TEM samples are prepared as ultra-thin sections, allowing for the direct observation of the individual particles without requiring a conductive coating, which enables a more accurate measurement of particle size. Figure 7c,d, at higher magnifications (20 nm and 10 nm, respectively), highlights the crystalline structure of the nanoparticles, with visible lattice fringes in Figure 7d indicating high crystallinity. The crystallites within the nanoparticles were between 20 and 60 nm in size, suggesting that each nanoparticle was composed of smaller crystalline domains. Furthermore, EDX analysis from TEM mapping (Figure 8) showed that the EDX analysis conducted during the TEM mapping, as shown in Figure 8, provided additional confirmation of the elemental composition of the CeO_2 nanoparticles. The EDX spectrum revealed distinct peaks for cerium (Ce) and oxygen (O), with not much significant evidence of impurities. The EDX elemental maps for Ce and O are shown in two different colors: green for Ce, and orange for O. These maps indicated a uniform distribution of cerium and oxygen across the nanoparticles, confirming that the CeO_2 nanoparticles were homogeneous in composition. The presence of less significant peaks of other elements in the EDX spectrum further supports the conclusion that the nanoparticles were composed predominantly of cerium and oxygen, in accordance with the expected CeO_2 structure.

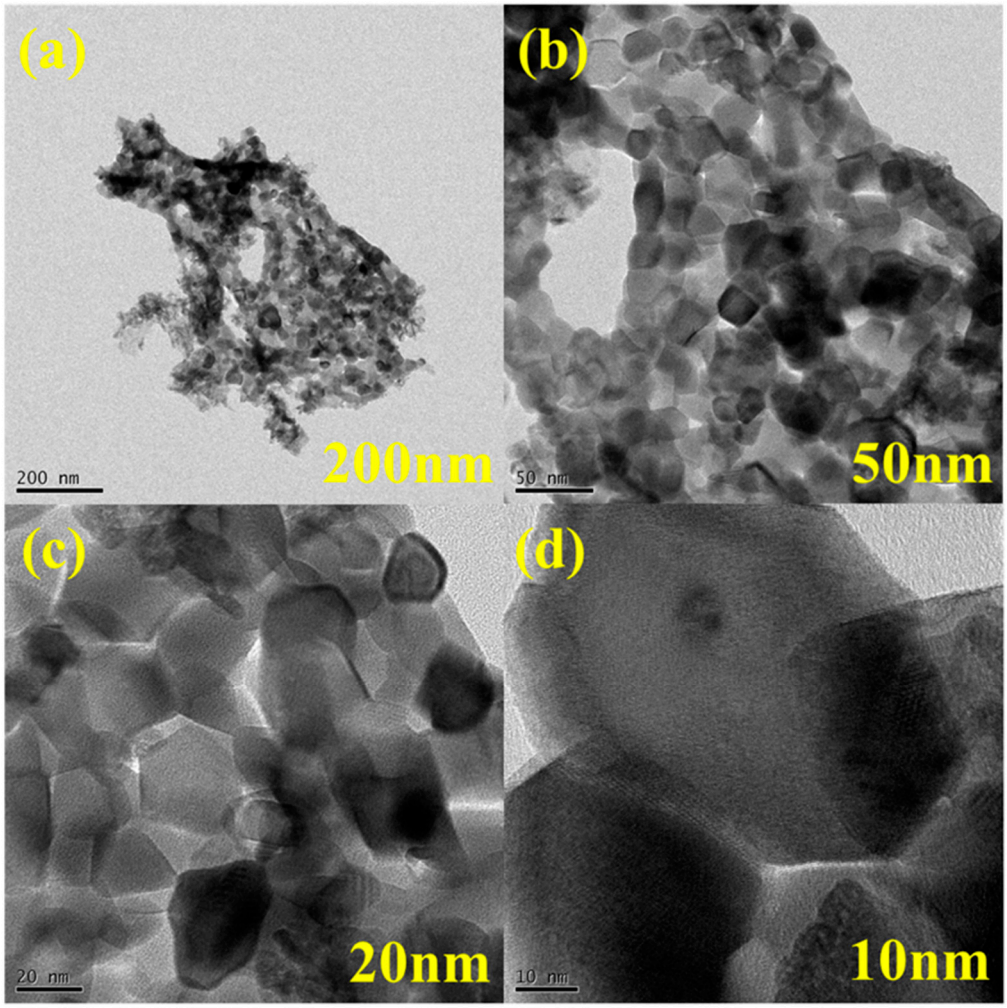

Figure 7. TEM morphology of CeO_2 nanoparticles at (**a**) 200 nm, (**b**) 50 nm, (**c**) 20 nm and (**d**) 10 nm scale.

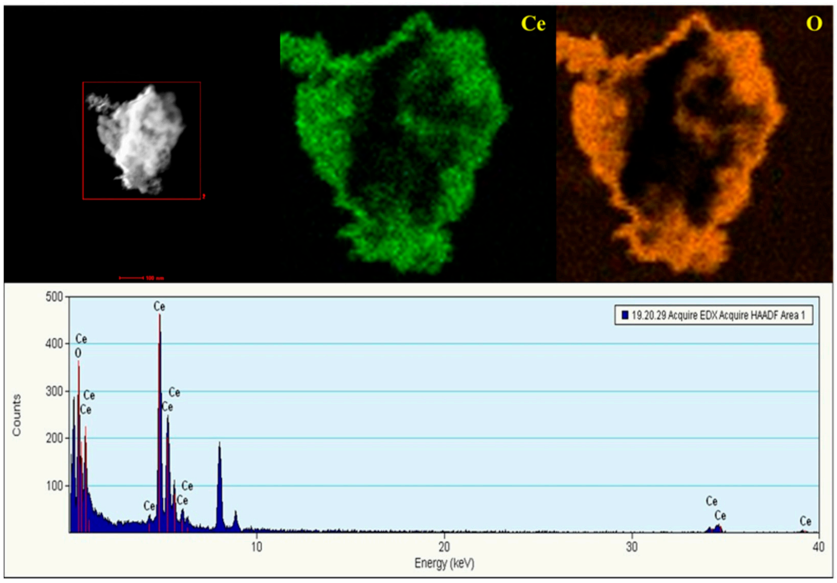

Figure 8. EDX taken from the TEM mapping of CeO_2 nanoparticles.

3.3. FTIR Characterization

The FTIR analysis of CeO_2 revealed a distinctive spectral profile, offering valuable insights into its molecular composition. As depicted in Figure 9, the spectrum exhibited key peaks at specific wavenumbers. A broad absorption band at 3396.09 cm^{-1} suggests the presence of hydroxyl groups, indicative of surface adsorption or structural hydroxyl moieties [38,48]. The peak at 1559.57 cm^{-1} corresponded to the symmetric stretching of oxygen within the Ce-O bond, confirming the oxide nature of the cerium compound. Additionally, peaks at 1318.34 cm^{-1} and 537.39 cm^{-1} can be attributed to lattice vibrations, further validating the crystalline structure of CeO_2. A notable peak at 1055 cm^{-1}, while less intense, may indicate C-O stretching or other minor functional groups present on the nanoparticle surface. The peaks observed between 537.39 cm^{-1} and 460.4 cm^{-1}, including those at 417.9 cm^{-1}, 413.79 cm^{-1}, 410.45 cm^{-1}, 407.19 cm^{-1}, and 403.7 cm^{-1}, are characteristic of metal-oxygen (M-O) stretching vibrations specific to Ce-O bonds [38]. These lower wavenumber peaks add to the comprehensive spectral data, reinforcing the structural and chemical properties of CeO_2 and confirming its purity and crystalline nature.

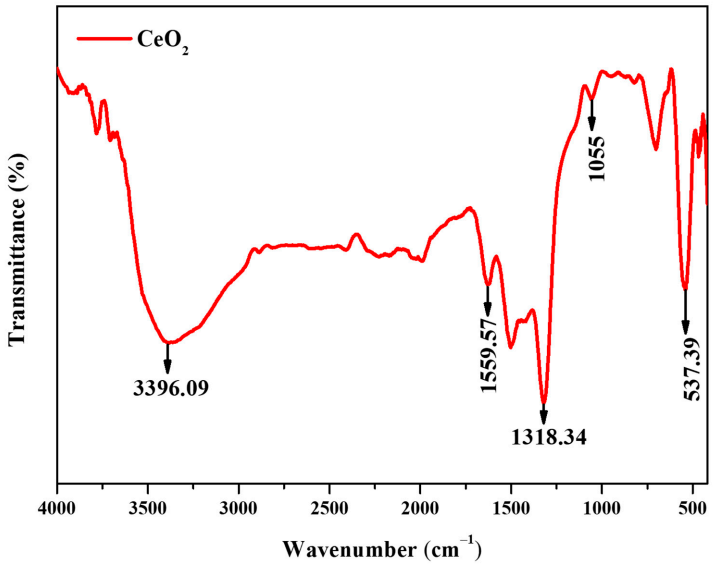

Figure 9. FTIR spectrum of CeO_2 nanoparticles.

3.4. TGA Analysis

The TGA graph illustrates the thermodynamic behavior of CeO_2 nanoparticles in a nitrogen-rich atmosphere. Figure 10 presents the relationship between weight loss and temperature as well as the derivative of the weight loss curve. The red curve represents the changes in sample mass, which can be attributed to thermal decomposition or oxidation processes. Concurrently, the black derivative weight curve reflects the rate of mass loss as a function of temperature. The CeO_2 nanoparticles displayed a noticeable weight loss, ranging from 100% to 94%, indicating thermal changes within this temperature range.

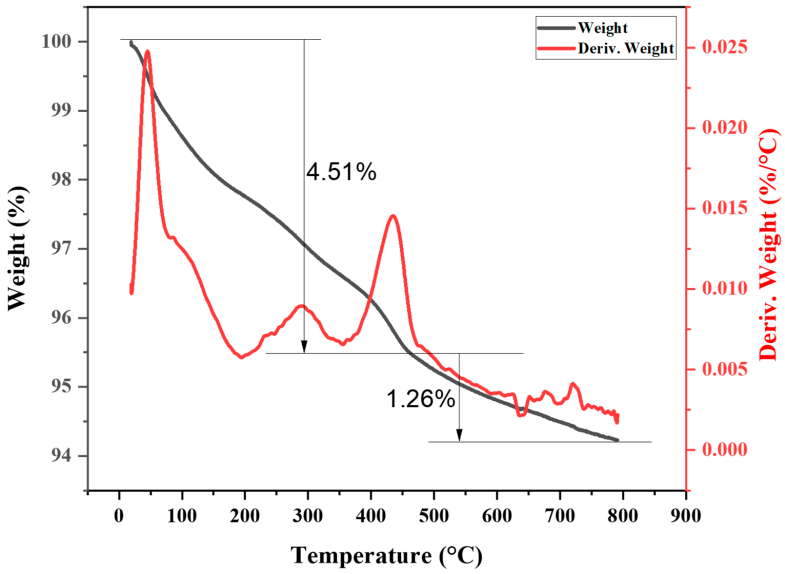

Figure 10. TGA graph of the prepared CeO_2 nanoparticles.

Between the temperatures of approximately 50 °C and 300 °C, a weight loss of 4.51% was observed. This weight loss was primarily attributed to the removal of surface-adsorbed water molecules or moisture from the nanoparticle surfaces, indicating a dehydration process. This phase marks the elimination of loosely bound water, which is a common characteristic of nanoparticles with a high surface area [49,50]. A second, more gradual weight loss of 1.26% occurred between 300 °C and 600 °C. This phase is associated with the slight decomposition of CeO_2 nanoparticles, most likely due to the loss of residual organic components or minor oxygen loss from the lattice structure of the nanoparticles [49]. This further reduction in weight indicates the onset of more stable thermal decomposition but remains minimal, demonstrating the excellent thermal stability of the biosynthesized CeO_2 nanoparticles. The derivative weight curve (red) showed two key peaks: one around 300 °C, corresponding to the initial weight loss phase (dehydration), and another smaller peak around 500 °C, indicating the completion of the minor thermal degradation [51]. The main peak near 300 °C is linked to the dehydration process, whereas the peak at 500 °C suggests additional thermal changes, possibly related to structural adjustments within the CeO_2 lattice [19]. The weight loss in the second phase, from 300 °C to 600 °C, was likely to be due to the slight decomposition of the CeO_2 lattice, which results in the release of oxygen. This phenomenon can be explained by the reduction of Ce^{4+} to Ce^{3+}, with oxygen loss from the lattice. The corresponding chemical equation for this process is as follows:

$$2CeO_2 \rightarrow Ce_2O_3 + \frac{1}{2}O_2$$

This equation represents the reduction of cerium oxide (CeO_2) to cerium(III) oxide (Ce_2O_3), accompanied by the release of oxygen (O_2). The minimal weight loss (1.26%) observed during this phase reflects the high thermal stability of the CeO_2 nanoparticles, as only a minor decomposition occurred, which is in line with the expectations for high-quality,

biosynthesized nanoparticles. The total weight loss of approximately 6% across the entire temperature range (from 50 °C to 800 °C) reflects the high thermal stability of the CeO_2 nanoparticles. When compared to previous studies [52] reporting weight losses of 12% or higher under similar conditions, the lower overall weight loss in this study highlights the superior thermal stability of the biosynthesized CeO_2 nanoparticles.

3.5. Zeta Potential

Zeta potential measurements were performed using the Zetasizer Nano ZS by Malvern Instruments (Almelo, The Netherlands) sourced from Central Equipment Center (Yeungnam University, Gyeongsan, Republic of Korea) to analyze the dispersion stability of the CeO_2-based nanolubricants. The zeta potential reflects the electrostatic interactions between particles in a suspension and is a key indicator of stability. Particles with high zeta potential values repel each other, preventing aggregation, while lower values suggest a tendency to cluster [53]. According to the literature, suspensions with a zeta potential greater than 30 mV are considered stable, those between 40 and 60 mV have good stability, and suspensions above 60 mV exhibit excellent stability [54]. Figure 11 presents the zeta potential values for all concentrations of nanolubricants tested. Based on the data, all nanolubricants exhibited zeta potential values exceeding 60 mV, indicating excellent stability. This suggests that the CeO_2 nanoparticles were well-dispersed in the PAO oil, with strong electrostatic repulsion forces between them. However, there were variations in the zeta potential values among the different concentrations. The 0.05 wt% and 0.15 wt% nanolubricants exhibited the highest zeta potential values at 75.2 mV and 81.4 mV, respectively. In contrast, the 0.1 wt% and 0.2 wt% nanolubricants showed lower zeta potential values of 68.9 mV and 65.2 mV, respectively. Variations in zeta potential among concentrations can be attributed to particle interactions. Higher concentrations may lead to closer particle packing and reduced electrostatic repulsion due to a thinner electrical double layer (EDL), thus lowering the zeta potential. The observed stability across all concentrations confirmed that the CeO_2 nanoparticles were well-dispersed in the PAO oil, with strong electrostatic repulsion maintaining the suspension's stability.

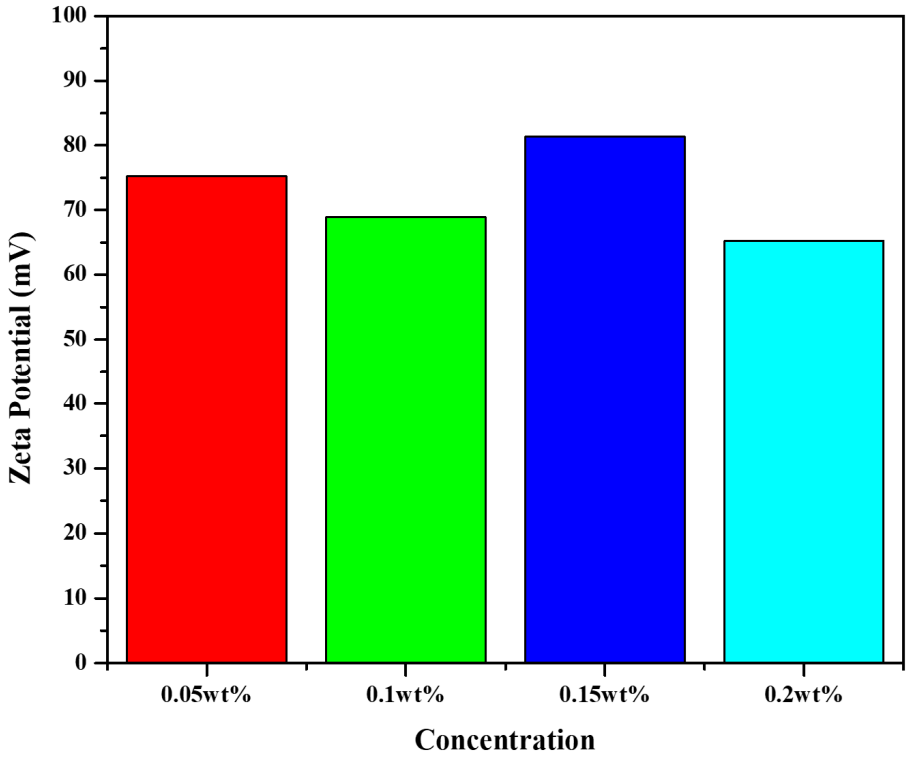

Figure 11. Zeta potential of various concentrations of nanolubricants.

3.6. Rheological Properties

The rheological properties of CeO_2-based nanolubricants dispersed in polyalpha-olefin (PAO) oil at various concentrations (0.05 wt%, 0.1 wt%, 0.15 wt%, and 0.2 wt%) were studied across four temperatures (40 °C, 60 °C, 80 °C, and 100 °C), as shown in Figure 12. The shear stress vs. shear rate plot (Figure 12a) demonstrated a positive linear relationship for all concentrations and temperatures, suggesting Newtonian-like behavior at lower shear rates and under moderate conditions [55,56]. At 40 °C, the highest shear stress values were observed, with the 0.2 wt% CeO_2 nanolubricant showing the greatest enhancement, attributed to the increased particle–particle and particle–fluid interactions [57]. Pure PAO oil exhibited the lowest shear stress response across all temperatures, highlighting the reinforcing effect of CeO_2 nanoparticles. As the temperatures increased to 60 °C, 80 °C, and 100 °C, a general decrease in shear stress values was noted due to thermal softening, which reduces fluid viscosity and decreases the energy required to shear the fluid. While all concentrations maintained higher shear stress values than pure PAO, the differences among them were less pronounced at higher temperatures.

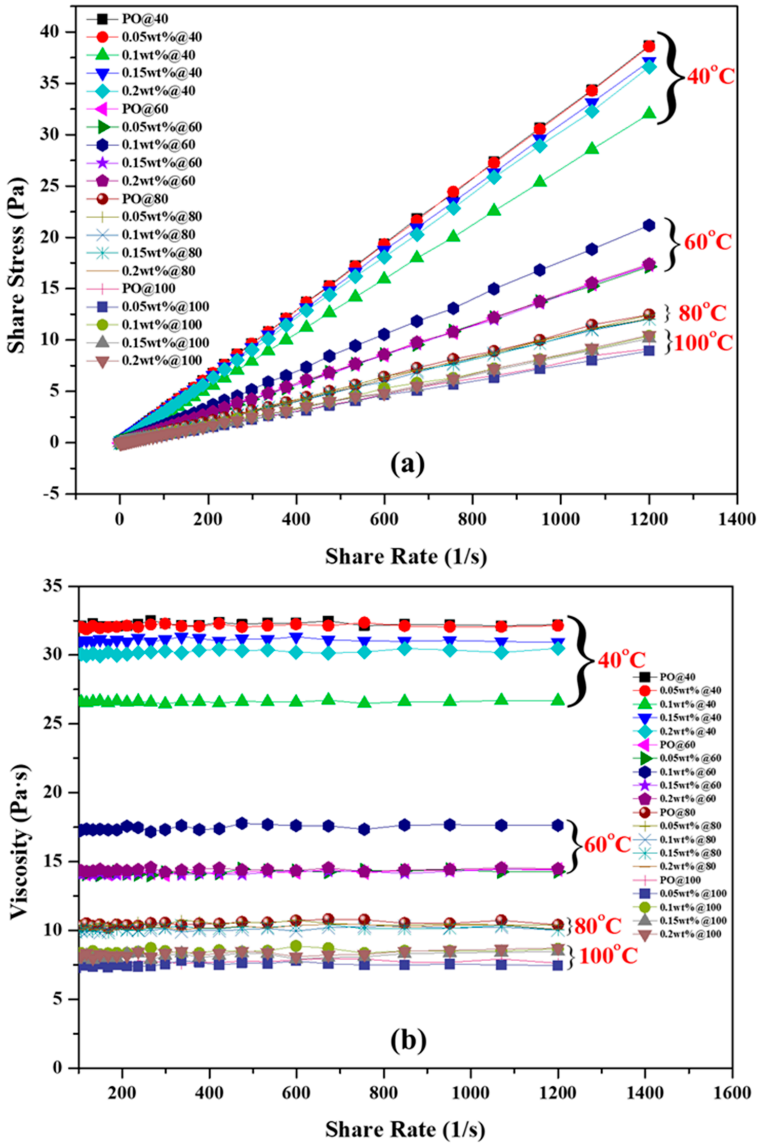

Figure 12. Shear stress (**a**) and viscosity (**b**) of pure oil (PO) and CeO_2-based nanolubricants at various concentrations (0.05, 0.1, 0.15, and 0.2 wt%) and temperatures (40 °C, 60 °C, 80 °C, and 100 °C) as a function of shear rate.

The viscosity vs. shear rate plot (Figure 12b) indicated a slight shear-thinning behavior for all nanolubricants, particularly at higher shear rates. This subtle decrease in viscosity with increasing shear rate is typical for nanolubricants and is desirable for high-shear applications as it reduces resistance to flow under high shear conditions [58]. At lower temperatures, the 0.2 wt% concentration exhibited higher viscosity compared to lower concentrations and pure PAO, which aligned with the expectations since the addition of CeO_2 nanoparticles forms a more structured network, increasing resistance to flow. The relatively stable viscosity at moderate shear rates suggests good nanoparticle dispersion. With elevated temperatures (60 °C, 80 °C, and 100 °C), the viscosity decreased across all samples due to the reduction in intermolecular forces and weakened nanoparticle–fluid interactions. Despite this decrease, the 0.2 wt% concentration maintained a higher viscosity than pure PAO, indicating resilience to temperature changes. All tested concentrations showed promising behavior across the temperature range, contributing to the potential for enhanced lubrication performance [59].

3.7. Viscosity Behavior and Temperature Dependency

The viscosity of fluids including nanolubricants with CeO_2 nanoparticles depends on various factors such as temperature, nanoparticle concentration, and molecular interactions. Typically, as the temperature rises, the viscosity of a fluid decreases due to the increase in kinetic energy, which weakens the intermolecular forces. However, the inclusion of nanoparticles introduces additional interactions that influence this behavior [52,60]. Figure 13 presents the combined analysis of the dynamic viscosity, relative viscosity, and viscosity index (VI) of CeO_2-based nanolubricants across various concentrations (0.05 wt%, 0.1 wt%, 0.15 wt%, and 0.2 wt%) and temperatures (40 °C, 60 °C, 80 °C, and 100 °C). As shown in Figure 13a, all tested nanolubricants exhibited a decrease in viscosity with increasing temperature, a trend characteristic of most fluids due to the reduction in intermolecular friction. At 40 °C, the 0.1 wt% concentration showed a significant initial viscosity (24.21 Pa·s) compared to the pure PAO oil (30.84 Pa·s), indicating enhanced nanoparticle interactions. However, as the temperature increased to 60 °C, all samples including the pure PAO displayed a sharp viscosity reduction, with the 0.1 wt% nanolubricant still maintaining a relatively higher viscosity. At 80 °C and 100 °C, the viscosities for all concentrations converged, suggesting that the temperature dominates viscosity behavior at higher temperatures. Figure 13b shows the relative viscosity of nanolubricants compared to the base PAO oil. Relative viscosity increases with nanoparticle concentration due to enhanced intermolecular interactions and the higher effective volume fraction in the fluid [61,62]. However, as the temperature rises, the relative viscosity decreases, reflecting reduced intermolecular forces and greater molecular mobility. The non-monotonic trends, such as the variations at 0.05 wt% between 40 °C and 100 °C, could be attributed to changes in dispersion and nanoparticle aggregation [63]. The VI, depicted in Figure 13c, indicates how fluid's viscosity changes with temperature. Higher VI values suggest better viscosity stability. The 0.1 wt% concentration achieved the highest VI, demonstrating improved temperature resilience, while the 0.05 wt% concentration had a lower VI than pure PAO, potentially due to weaker interactions or nanoparticle settling. The increased VI in other concentrations was likely due to the structural changes induced by CeO_2 nanoparticles, which form interactions such as hydrogen bonds or dipole–dipole forces that enhance the viscosity–temperature relationship [63–65].

The combined analysis in Figure 13 highlights that CeO_2 nanoparticles can improve the viscosity behavior and thermal stability of PAO oil, particularly at lower to moderate temperatures. However, as the temperature increased, the effect of nanoparticle concentration diminished, making the fluid's inherent properties more influential. Selecting the appropriate concentration is essential for optimizing the nanolubricant performance across a range of operating temperatures.

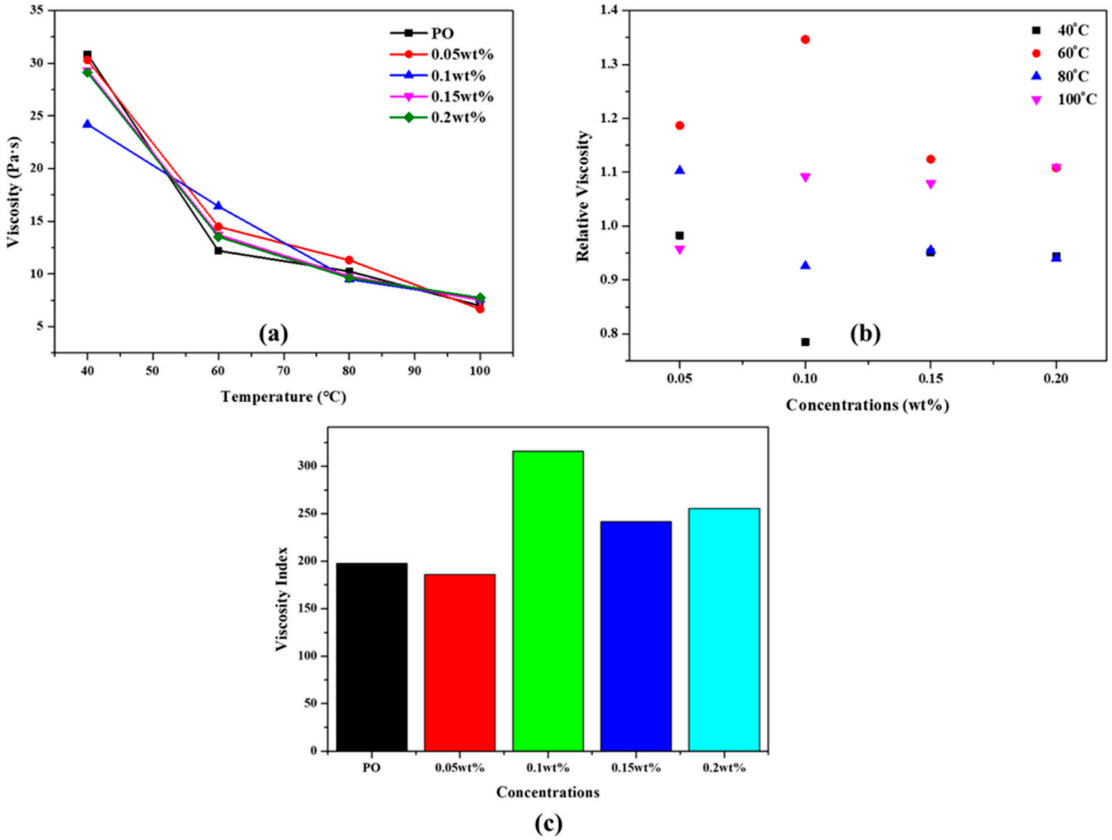

Figure 13. Viscosity behavior of CeO_2 nanolubricants at various concentrations and temperatures. (**a**) Dynamic viscosity, (**b**) relative viscosity, and (**c**) viscosity index (VI) of nanolubricants compared to the pure PAO oil.

3.8. Thermal Conductivity Analysis

The examination of heat conduction properties in nanolubricants containing CeO_2 nanoparticles demonstrated improved heat transfer capabilities. As shown in Figure 14, there was a consistent increase in thermal conductivity with rising nanoparticle concentrations, except for the 0.1 wt% sample, which showed a lower value compared to the 0.05 wt% sample. This slight decrease could be attributed to nanoparticle agglomeration at higher concentrations, which reduces the effective surface area for contact and heat transfer between the nanoparticles and base oil [61]. The error bars presented in Figure 14 provide valuable insights into the variability of the measurements across different concentrations. For instance, the error margin was notably higher for the 0.05 wt% and 0.2 wt% concentrations, indicating some variability in thermal conductivity values, potentially due to differences in nanoparticle dispersion. This suggests that while CeO_2 nanoparticles enhance thermal conductivity overall, maintaining uniform nanoparticle dispersion is essential to achieve consistent performance across different tests. Despite the observed variability, the most significant improvement in thermal conductivity was observed with the 0.2 wt% sample, reaching 0.12 W/mK—an approximate 43% increase compared to the base oil (PO), which had a value of 0.05 W/mK. The enhancement in thermal conductivity due to CeO_2 nanoparticles can be explained by several factors including their inherently high thermal conductivity, the formation of a conductive network within the nanolubricant, and increased convection driven by the Brownian motion of the nanoparticles. Other influential parameters include nanoparticle size, shape, surface modification, base oil type and viscosity as well as the temperature and shear rate of the nanolubricant [66]. This highlights that incorporating CeO_2 nanoparticles into PAO oil-based nanolubricants significantly boosts their thermal conductivity at various concentrations.

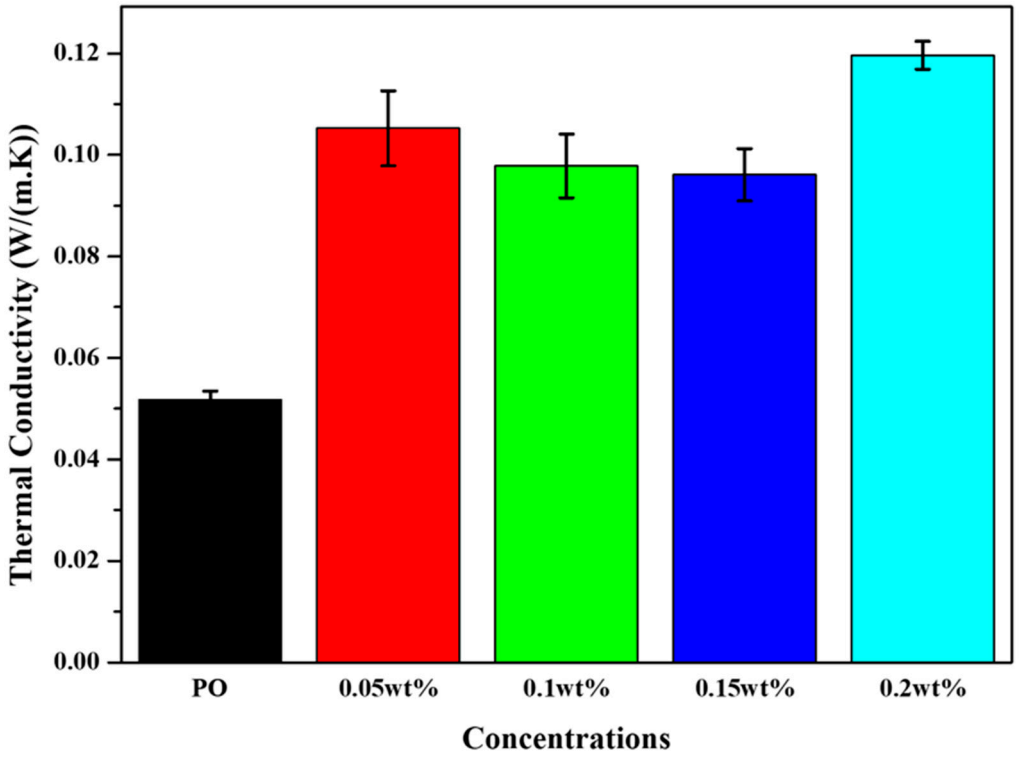

Figure 14. Thermal conductivity of various concentrations of nanolubricants.

3.9. Tribological Properties

In this study, a reciprocating tribometer was employed to measure the coefficient of friction (CoF) of both the pure oil (PO) and nanolubricants formulated with polyalphaolefin (PAO) oil as the base and CeO_2 nanoparticles as additives. The nanolubricants were prepared with varying CeO_2 concentrations (0.05, 0.1, 0.15, and 0.2 wt%), and each test was performed three times to ensure data accuracy. The tribometer was run over a sliding distance of 840 m, with data points representing the average CoF recorded every 40 m, as presented in Figure 15. To eliminate potential confusion from transient fluctuations observed at the beginning of each test, only the stable portion of the friction data is presented. During the initial stage, minor disturbances in the CoF were observed as the test setup stabilized; these effects dissipated over time, leading to consistent and reliable data. The error bars in the new figure illustrate the variability in CoF over the sliding distance, with the standard deviations for the PO, 0.05 wt%, 0.1 wt%, 0.15 wt%, and 0.2 wt% CeO_2 nanolubricants being 0.00592, 0.0042, 0.00782, 0.00975, and 0.00869, respectively. These values reflect the consistency and reliability of the results, with lower standard deviations, such as that for 0.05 wt% and PO, indicating more stable CoF values across the entire test. The 0.15 wt% concentration continued to exhibit the lowest CoF, reinforcing its optimal friction-reducing performance. The results clearly indicate that the CoF of pure PO was consistently higher than that of the CeO_2-based nanolubricants across all distances and concentrations, demonstrating that the addition of CeO_2 nanoparticles significantly reduced the friction between sliding surfaces. Several mechanisms may account for this friction reduction. First, the formation of a protective tribofilm on the surface, facilitated by the catalytic activity of CeO_2 nanoparticles [52,67], plays a critical role. This tribofilm can minimize surface roughness and prevent direct metal-to-metal contact, effectively lowering the CoF. Second, the spherical morphology of CeO_2 nanoparticles can contribute to a rolling effect [68]. These nanoparticles act like nanoscale ball bearings, reducing the contact area between surfaces and further decreasing friction. Another contributing factor is the polishing effect of CeO_2 nanoparticles [52], where the nanoparticles smooth out surface asperities and remove wear debris, thus lowering the CoF even more. The data also revealed the

concentration dependent behavior of the CoF. As the concentration of CeO_2 nanoparticles increased, the CoF decreased, reaching its lowest value at 0.15 wt%. However, a slight increase in CoF was observed at 0.2 wt%, suggesting that there is an optimal concentration of CeO_2 nanoparticles for minimizing friction. Several factors could explain this trend. First, the dispersion stability of the nanolubricants is critical. At higher concentrations, CeO_2 nanoparticles may tend to agglomerate or settle, reducing their effectiveness in lowering friction [69]. Second, as the concentration increases, the viscosity of the nanolubricants also rises due to intensified interparticle interactions, which could increase the fluid resistance and thereby raise the CoF [67]. Additionally, the balance between tribofilm formation and removal must be considered. While higher concentrations of CeO_2 nanoparticles promote greater tribofilm formation due to increased catalytic activity [18], they may also enhance the polishing effect, leading to the faster removal of the tribofilm. This creates a trade-off between tribofilm formation and removal, influencing the overall CoF [70,71]. In conclusion, this experiment demonstrates that incorporating CeO_2 nanoparticles into PAO oil effectively reduces friction, making it a promising additive for lubricant applications. The nanolubricant with a 0.15 wt% concentration of CeO_2 nanoparticles achieved the lowest friction coefficient, showing an approximate 26% reduction compared to the base oil. This friction reduction is likely due to a combination of factors including the formation of a protective tribofilm, the rolling and polishing effects of CeO_2 nanoparticles, stable dispersion, and balanced interaction between viscosity and tribofilm dynamics. The relatively low standard deviation values across all concentrations support the consistency and reliability of the tribological performance observed. These insights highlight the potential of CeO_2 nanoparticles to significantly enhance the tribological performance of lubricants.

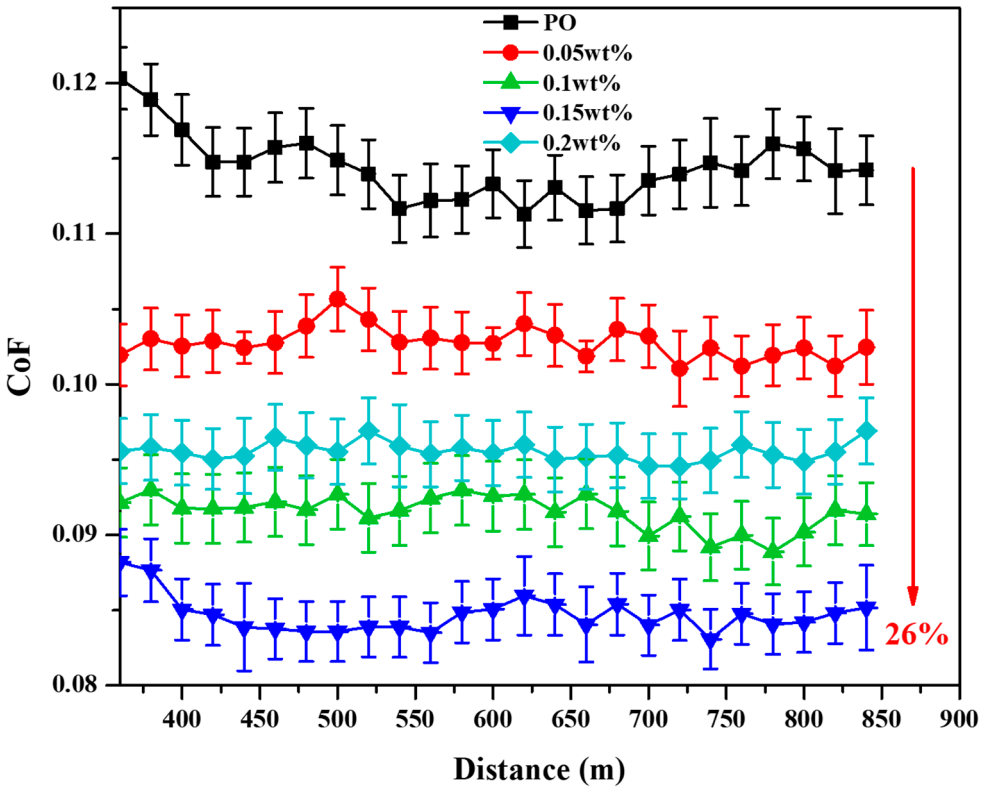

Figure 15. Coefficient of friction of various concentrations of nanolubricants.

3.10. Wear Analysis

The wear tracks were analyzed using the NANOSCOPE NS-3500 (Dallas, TX, USA), a high-speed confocal laser scanning microscope (CLSM) designed for precise three-dimensional (3D) measurements. This instrument captures real-time confocal microscopic images using advanced optical scanning modules and sophisticated signal processing

algorithms. The wear tracks generated by the tribometer were examined in both 3D and 2D profiles, as shown in Figure 16. The 3D surface topography provides an in-depth view of the wear tracks, capturing details of surface texture and irregularities caused by friction, while the 2D profiles provide precise cross-sectional data. These detailed wear profiles are essential for accurately quantifying the wear volume and calculating specific wear rates. The roughness parameters extracted from these profiles include the maximum mean height (Ra), root mean square deviation (Rq), skewness (Rsk), kurtosis (Rk), maximum peak height (Rp), maximum profile valley depth (Rv), and total profile height (Rt). These results, plotted in Figure 17, demonstrate that the best roughness parameters were obtained at the 0.15 wt% concentration, consistent with the CoF results, which also indicated the maximum friction reduction at this concentration compared to the others.

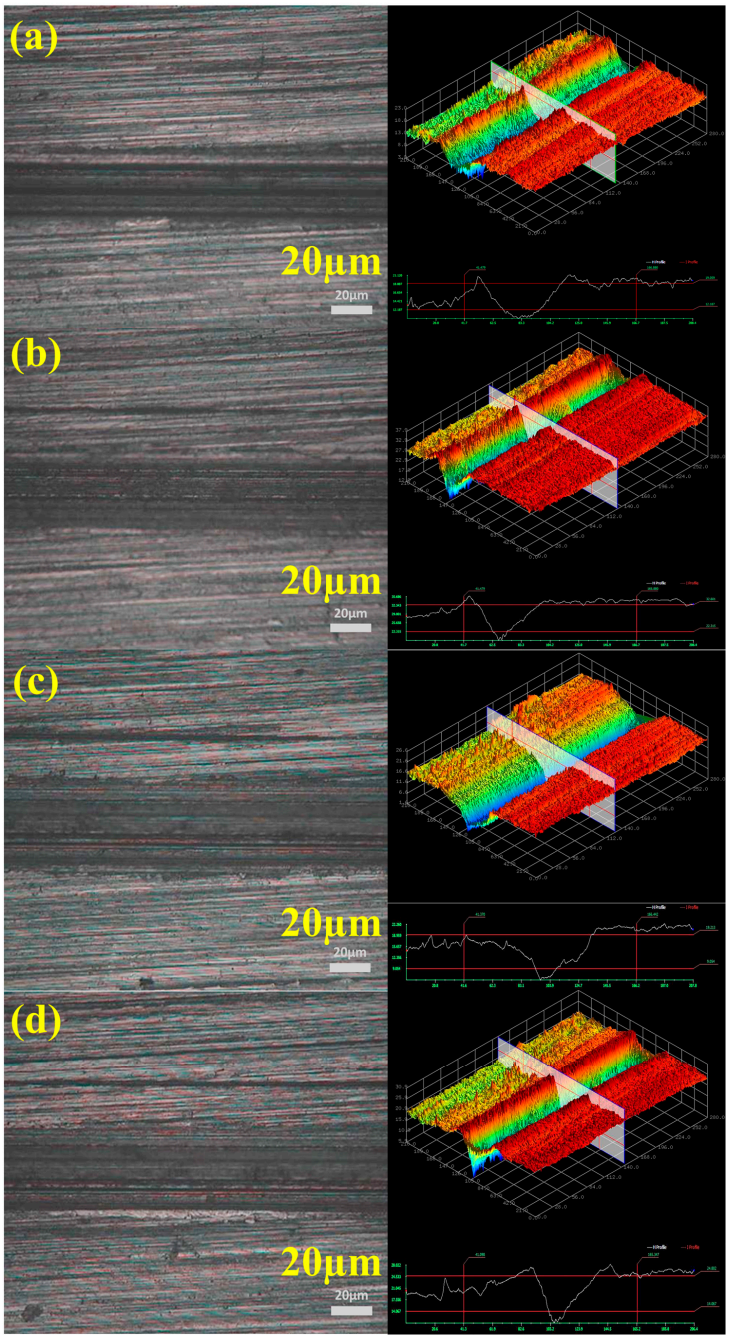

Figure 16. Wear tracks of the (**a**) 0.05 wt%, (**b**) 0.1 wt%, (**c**) 0.15 wt%, and (**d**) 0.2 wt% concentrations used in the tribometer tests.

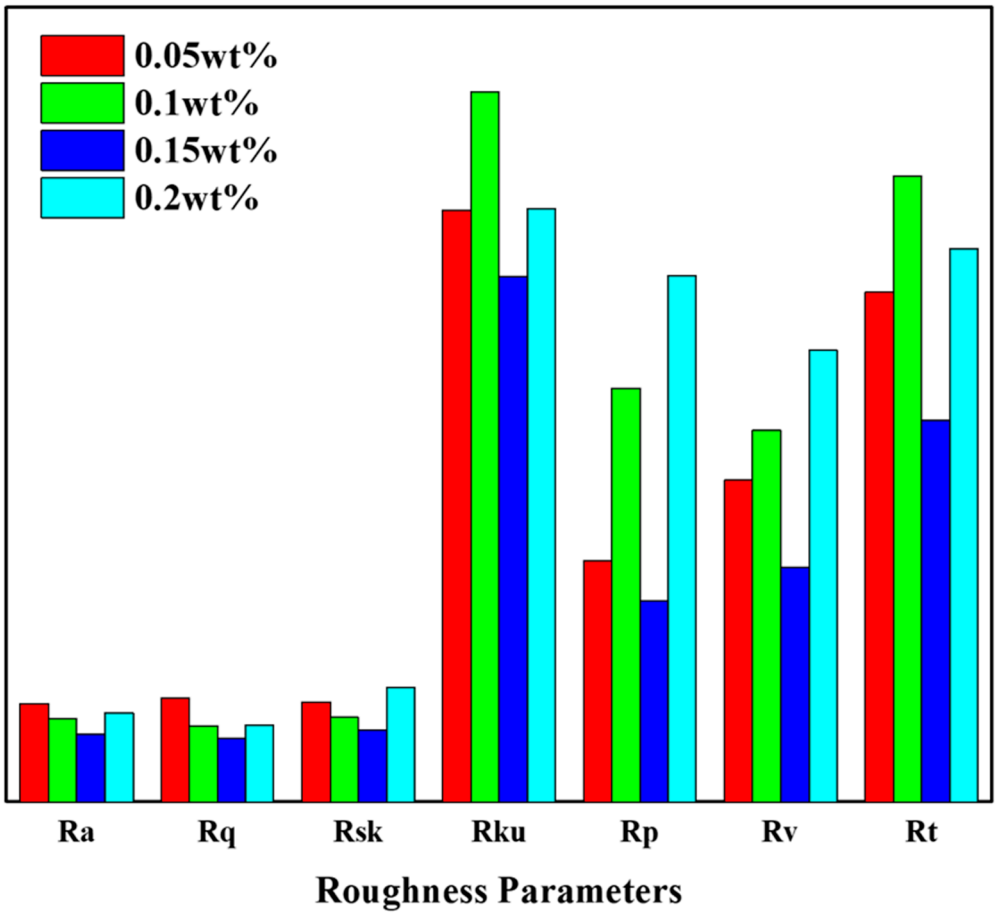

Figure 17. Roughness parameters of the wear tracks associated with each concentration.

The data from the 2D profiles in Figure 16 were further analyzed to determine the wear volume. The wear volume was assessed using ImageJ 1.54d software, which processed the 2D profile data provided by the NANOSCOPE. The specific wear rate (SWR) was calculated by multiplying the area measured with ImageJ by the wear track length to derive the wear volume, then applying the Archard equation [72]. The SWR, which quantifies the material loss per unit sliding distance and applied load, provides an indication of wear resistance, with lower SWR values signifying superior performance. As shown in Figure 18, the SWR of pure oil (PO) was significantly higher at 4.621 mm^3/Nm compared to all of the nanolubricants. This clearly demonstrates the beneficial effect of adding CeO_2 nanoparticles to PAO oil in reducing wear. The wear rate progressively decreased as the concentration of CeO_2 nanoparticles increased from 0.05 wt% to 0.15 wt%, reaching the lowest SWR of 2.408 mm^3/Nm at 0.15 wt%. This indicates that the 0.15 wt% concentration provided the optimal anti-wear performance by forming a protective tribofilm [52,73], reducing metal-to-metal contact, and minimizing material loss. However, at the 0.2 wt% concentration, the SWR increased slightly to 3.19 mm^3/Nm, suggesting that higher concentrations of CeO_2 nanoparticles may act as abrasive particles, leading to increased wear [74]. Therefore, controlling the concentration of CeO_2 nanoparticles is crucial for optimizing tribological performance. The inclusion of CeO_2 nanoparticles at a concentration of 0.15 wt% achieved the best balance between forming a protective tribofilm and minimizing abrasive wear, yielding the lowest SWR and superior wear resistance. The relatively low standard deviation values across all concentrations underscore the consistency and reliability of the observed tribological performance.

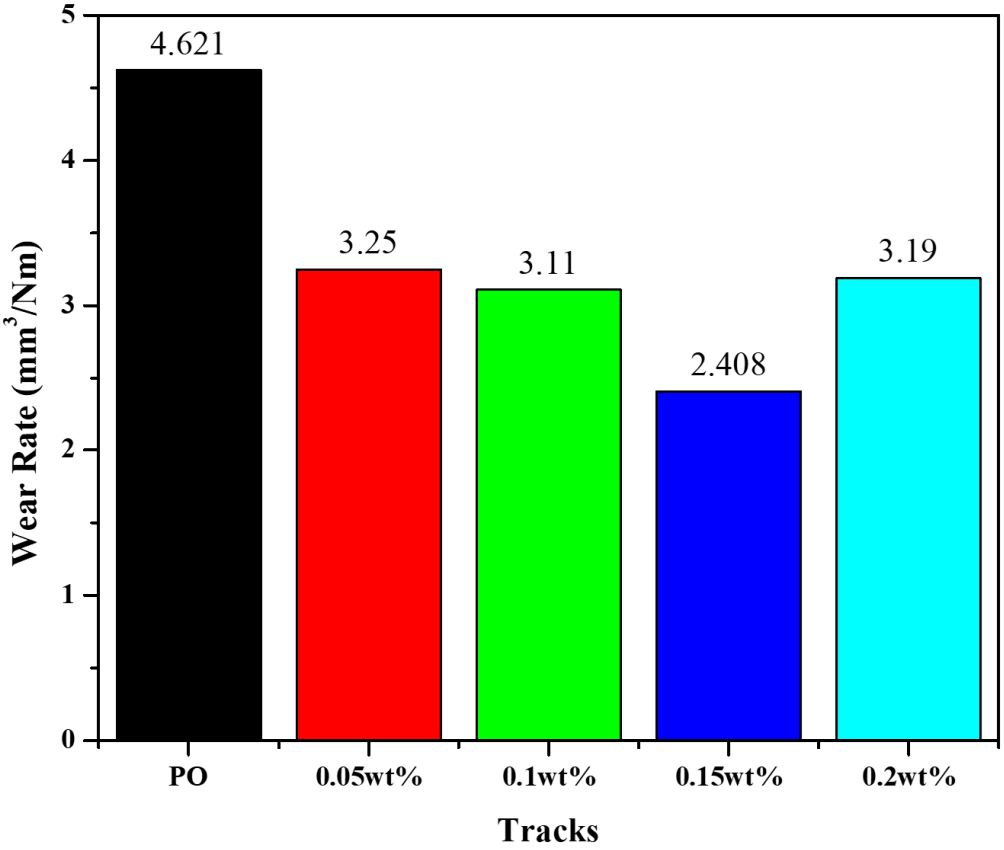

Figure 18. Specific wear rate obtained on each track.

4. Conclusions

This study highlights the promising potential of biosynthesized CeO_2 nanoparticles as highly effective additives in polyalphaolefin (PAO)-based nanolubricants. The nanoparticles were synthesized using an environmentally friendly biosynthesis process with Moringa oleifera leaf extract, offering a sustainable and green alternative to conventional chemical methods. This approach not only reduces the environmental impact, but also enhances the nanoparticle properties, as confirmed by XRD and TEM, which demonstrated excellent thermal stability, with only 6% weight loss observed during TGA. The inclusion of CeO_2 nanoparticles led to substantial improvements in the thermal, rheological, and tribological performance of the nanolubricants. The 0.15 wt% concentration proved to be the most effective, showing shear-thinning behavior and achieving the optimal viscosity reduction, making it particularly suitable for lubrication at moderate temperatures. The high zeta potential of 81.4 mV further confirmed the excellent dispersion stability of the nanolubricants, ensuring minimal nanoparticle aggregation. Thermal conductivity tests showed a 43% improvement, significantly enhancing the heat transfer capabilities of the oil. Moreover, tribological tests revealed that the 0.15 wt% CeO_2 nanolubricant exhibited the lowest coefficient of friction, showing an approximate 26% reduction compared to the base oil, along with a notable decrease in specific wear rate, reflecting superior anti-friction and anti-wear properties. The biosynthesized CeO_2 nanoparticles not only improved the performance of the lubricant, but also promoted a more sustainable and eco-friendly production process. The 0.15 wt% concentration emerged as the optimal formulation, offering a balanced combination of nanoparticle dispersion, tribofilm formation, and viscosity reduction. These findings underscore the potential of CeO_2 nanoparticles synthesized through green biosynthesis for developing advanced, environmentally conscious lubricants with better stability, thermal efficiency, and wear resistance.

Author Contributions: Conceptualization, S.A. and S.-S.P.; Methodology, S.A.; Software, S.A.; Validation, S.-S.P.; Formal analysis, S.-S.P.; Investigation, S.-S.P.; Resources, S.-S.P.; Data curation, S.A.; Writing—original draft preparation, S.A.; Writing—review and editing, S.-S.P.; Visualization, S.A.; supervision, S.-S.P.; Funding acquisition, S.-S.P. All authors have read and agreed to the published version of the manuscript.

Funding: This research received no external funding.

Data Availability Statement: Data are unavailable due to privacy or ethical restrictions.

Conflicts of Interest: The authors declare no conflicts of interest.

References

1. Singh, Y.; Kumar Singh, N.; Sharma, A.; Singla, A.; Singh, D.; Abd Rahim, E. Effect of ZnO nanoparticles concentration as additives to the epoxidized Euphorbia Lathyris oil and their tribological characterization. *Fuel* **2021**, *285*, 119148. [CrossRef]
2. Tijerina, J.T.; Castillo, F.; Leal, J.; Parás, L.P.; Cortés, D.M.; Cruz, C.; García, G.G.; García, P. Nanoparticles of Zn and ZnO as extreme pressure (EP) additives for lubricants. *J. Appl. Res. Technol.* **2019**, 16. [CrossRef]
3. Vardhaman, B.S.A.; Amarnath, M.; Ramkumar, J.; Mondal, K. Enhanced tribological performances of zinc oxide/MWCNTs hybrid nanomaterials as the effective lubricant additive in engine oil. *Mater. Chem. Phys.* **2020**, *253*, 123447. [CrossRef]
4. Navada, M.K.; Rai, R.; Ganesha, A.; Patil, S. Synthesis and characterization of size controlled nano copper oxide structures for antioxidant study and as eco-friendly lubricant additive for bio-oils. *Ceram. Int.* **2023**, *49*, 10402–10410. [CrossRef]
5. Azam, S.; Park, S.-S. Sonochemical Synthesis of CuO Nanoplatelets and Their Tribological Properties as an Additive in Synthetic Oil Using Reciprocating Tribometer. *Lubricants* **2023**, *11*, 185. [CrossRef]
6. Ingole, S.; Charanpahari, A.; Kakade, A.; Umare, S.S.; Bhatt, D.V.; Menghani, J. Tribological behavior of nano TiO_2 as an additive in base oil. *Wear* **2013**, *301*, 776–785. [CrossRef]
7. Birleanu, C.; Pustan, M.; Cioaza, M.; Molea, A.; Popa, F.; Contiu, G. Effect of TiO_2 nanoparticles on the tribological properties of lubricating oil: An experimental investigation. *Sci. Rep.* **2022**, *12*, 5201. [CrossRef]
8. Kulkarni, T.; Toksha, B.; Autee, A. Optimizing nanoparticle attributes for enhanced anti-wear performance in nano-lubricants. *J. Eng. Appl. Sci.* **2024**, *71*, 30. [CrossRef]
9. Lu, Z.; Lin, Q.; Cao, Z.; Li, W.; Gong, J.; Wang, Y.; Hu, K.; Hu, X. MoS_2 Nanomaterials as Lubricant Additives: A Review. *Lubricants* **2023**, *11*, 527. [CrossRef]
10. Gao, Z.; Nie, W.; Wang, H.; Ren, S.; Du, D.; Du, S.; Li, J. Enhancing mechanical performance and high-temperature lubrication enabled by MoS2/WB2 nanolayered films. *Compos. Part B Eng.* **2024**, *275*, 111350. [CrossRef]
11. Chen, J.; He, K.; Fei, J.; Yu, J.; Meng, Z.; Pang, Y.; Liang, L.; Tian, Z.Q. Extreme pressure and anti-wear properties of polycarboxylate superplasticizer modified 3D porous graphene/SiO_2 as water-based lubricant additives. *Wear* **2024**, *540–541*, 205239. [CrossRef]
12. He, Q.; Li, A.; Guo, Y.; Liu, S.; Kong, L.-H. Effect of nanometer silicon dioxide on the frictional behavior of lubricating grease. *Nanomater. Nanotechnol.* **2017**, *7*, 1847980417725933. [CrossRef]
13. Jin, B.; Chen, G.; He, Y.; Zhang, C.; Luo, J. Lubrication properties of graphene under harsh working conditions. *Mater. Today Adv.* **2023**, *18*, 100369. [CrossRef]
14. Marlinda, A.R.; Thien, G.S.; Shahid, M.; Ling, T.Y.; Hashem, A.; Chan, K.-Y.; Johan, M.R. Graphene as a Lubricant Additive for Reducing Friction and Wear in Its Liquid-Based Form. *Lubricants* **2023**, *11*, 29. [CrossRef]
15. Zhang, H.; Mo, Y.; Lv, J.; Wang, J. Tribological Behavior of WS2 Nanoparticles as Additives in Calcium Sulfonate Complex–Polyurea Grease. *Lubricants* **2023**, *11*, 259. [CrossRef]
16. Freschi, M.; Di Virgilio, M.; Zanardi, G.; Mariani, M.; Lecis, N.; Dotelli, G. Employment of Micro- and Nano-WS2 Structures to Enhance the Tribological Properties of Copper Matrix Composites. *Lubricants* **2021**, *9*, 53. [CrossRef]
17. Othman, A.; Gowda, A.; Andreescu, D.; Hassan, M.H.; Babu, S.V.; Seo, J.; Andreescu, S. Two decades of ceria nanoparticle research: Structure, properties and emerging applications. *Mater. Horiz.* **2024**, *11*, 3213–3266. [CrossRef]
18. Lei, X.; Zhang, Y.; Zhang, S.; Yang, G.; Zhang, C.; Zhang, P. Study on the mechanism of rapid formation of ultra-thick tribofilm by CeO2 nano additive and ZDDP. *Friction* **2023**, *11*, 48–63. [CrossRef]
19. Yadav, N. Cerium oxide nanostructures: Properties, biomedical applications and surface coatings. *3 Biotech* **2022**, *12*, 121. [CrossRef]
20. Yi, L.; Yu, L.; Chen, S.; Huang, D.; Yang, C.; Deng, H.; Hu, Y.; Wang, H.; Wen, Z.; Wang, Y.; et al. The regulatory mechanisms of cerium oxide nanoparticles in oxidative stress and emerging applications in refractory wound care. *Front. Pharmacol.* **2024**, *15*, 1439960. [CrossRef]
21. Song, G.; Cheng, N.; Zhang, J.; Huang, H.; Yuan, Y.; He, X.; Luo, Y.; Huang, K. Nanoscale Cerium Oxide: Synthesis, Biocatalytic Mechanism, and Applications. *Catalysts* **2021**, *11*, 1123. [CrossRef]
22. Singh, K.R.; Nayak, V.; Sarkar, T.; Singh, R.P. Cerium oxide nanoparticles: Properties, biosynthesis and biomedical application. *RSC Adv.* **2020**, *10*, 27194–27214. [CrossRef] [PubMed]
23. Younis, A.; Chu, D.; Li, S. *Cerium Oxide Nanostructures and Their Applications*; Farrukh, M.A., Ed.; IntechOpen: Rijeka, Croatia, 2016; Chapter 3; ISBN 978-953-51-2856-4.

24. Pena-Paras, L.; Maldonado-Cortes, D.; Taha-Tijerina, J.; Irigoyen, M.; Guerra, J. Experimental evaluation of the tribological behaviour of CeO2 nanolubricants under extreme pressures. *IOP Conf. Ser. Mater. Sci. Eng.* **2018**, *400*, 72003. [CrossRef]
25. GU, C.; LI, Q.; GU, Z.; ZHU, G. Study on application of CeO_2 and $CaCO_3$ nanoparticles in lubricating oils. *J. Rare Earths* **2008**, *26*, 163–167. [CrossRef]
26. Pundir, S.; Priya, R.; Singh, K.; Kaur, H.; Choudhary, P. A systematic study on synthesis of CeO_2 nanoparticles by various routes. *IOP Conf. Ser. Earth Environ. Sci.* **2023**, *1110*, 012030. [CrossRef]
27. Selvan, R.K.; Augustin, C.O.; Šepelák, V.; Berchmans, L.J.; Sanjeeviraja, C.; Gedanken, A. Synthesis and characterization of $CuFe_2O_4/CeO_2$ nanocomposites. *Mater. Chem. Phys.* **2008**, *112*, 373–380. [CrossRef]
28. Malleshappa, J.; Nagabhushana, H.; Prasad, B.D.; Sharma, S.C.; Vidya, Y.S.; Anantharaju, K.S. Structural, photoluminescence and thermoluminescence properties of CeO_2 nanoparticles. *Optik* **2016**, *127*, 855–861. [CrossRef]
29. Aruna, S.T.; Kini, N.S.; Rajam, K.S. Solution combustion synthesis of CeO_2–$CeAlO_3$ nano-composites by mixture-of-fuels approach. *Mater. Res. Bull.* **2009**, *44*, 728–733. [CrossRef]
30. Avgouropoulos, G.; Ioannides, T. Selective CO oxidation over CuO-CeO_2 catalysts prepared via the urea–nitrate combustion method. *Appl. Catal. A Gen.* **2003**, *244*, 155–167. [CrossRef]
31. Xiong, J.-Q.; Ru, S.; Zhang, Q.; Jang, M.; Kurade, M.B.; Kim, S.-H.; Jeon, B.-H. Insights into the effect of cerium oxide nanoparticle on microalgal degradation of sulfonamides. *Bioresour. Technol.* **2020**, *309*, 123452. [CrossRef]
32. Kannan, S.K.; Sundrarajan, M. A Green Approach for the Synthesis of a Cerium Oxide Nanoparticle: Characterization and Antibacterial Activity. *Int. J. Nanosci.* **2014**, *13*, 1450018. [CrossRef]
33. Darroudi, M.; Hoseini, S.J.; Kazemi Oskuee, R.; Hosseini, H.A.; Gholami, L.; Gerayli, S. Food-directed synthesis of cerium oxide nanoparticles and their neurotoxicity effects. *Ceram. Int.* **2014**, *40*, 7425–7430. [CrossRef]
34. Dutta, D.; Mukherjee, R.; Patra, M.; Banik, M.; Dasgupta, R.; Mukherjee, M.; Basu, T. Green synthesized cerium oxide nanoparticle: A prospective drug against oxidative harm. *Colloids Surf. B Biointerfaces* **2016**, *147*, 45–53. [CrossRef] [PubMed]
35. Gong, D.; Celi, N.; Zhang, D.; Cai, J. Magnetic Biohybrid Microrobot Multimers Based on Chlorella Cells for Enhanced Targeted Drug Delivery. *ACS Appl. Mater. Interfaces* **2022**, *14*, 6320–6330. [CrossRef]
36. Naveed, M.; Makhdoom, S.I.; Rehman, S.U.; Aziz, T.; Bashir, F.; Ali, U.; Alharbi, M.; Alshammari, A.; Alasmari, A.F. Biosynthesis and Mathematical Interpretation of Zero-Valent Iron NPs Using Nigella sativa Seed Tincture for Indemnification of Carcinogenic Metals Present in Industrial Effluents. *Molecules* **2023**, *28*, 3299. [CrossRef]
37. Aseyd Nezhad, S.; Es-haghi, A.; Tabrizi, M.H. Green synthesis of cerium oxide nanoparticle using Origanum majorana L. leaf extract, its characterization and biological activities. *Appl. Organomet. Chem.* **2020**, *34*, e5314. [CrossRef]
38. Tumkur, P.P.; Gunasekaran, N.K.; Lamani, B.R.; Nazario Bayon, N.; Prabhakaran, K.; Hall, J.C.; Ramesh, G.T. Cerium Oxide Nanoparticles: Synthesis and Characterization for Biosafe Applications. *Nanomanufacturing* **2021**, *1*, 176–189. [CrossRef]
39. Eka Putri, G.; Rilda, Y.; Syukri, S.; Labanni, A.; Arief, S. Highly antimicrobial activity of cerium oxide nanoparticles synthesized using Moringa oleifera leaf extract by a rapid green precipitation method. *J. Mater. Res. Technol.* **2021**, *15*, 2355–2364. [CrossRef]
40. Jayakumar, G.; Albert Irudayaraj, A.; Dhayal Raj, A. A comprehensive investigation on the properties of nanostructured cerium oxide. *Opt. Quantum Electron.* **2019**, *51*, 312. [CrossRef]
41. Miri, A.; Sarani, M.; Khatami, M. Nickel-doped cerium oxide nanoparticles: Biosynthesis, cytotoxicity and UV protection studies. *RSC Adv.* **2020**, *10*, 3967–3977. [CrossRef]
42. Ioannou, M.E.; Pouroutzidou, G.K.; Chatzimentor, I.; Tsamesidis, I.; Florini, N.; Tsiaoussis, I.; Lymperaki, E.; Komninou, P.; Kontonasaki, E. Synthesis and Characterization of Cerium Oxide Nanoparticles: Effect of Cerium Precursor to Gelatin Ratio. *Appl. Sci.* **2023**, *13*, 2676. [CrossRef]
43. González de Arrieta, I.; del Campo, L.; De Sousa Meneses, D. Infrared spectroscopy of CeO2 nanoparticles using Bergman's spectral representation: Effects of phonon confinement and lattice strain. *Phys. Chem. Chem. Phys.* **2021**, *23*, 13095–13105. [CrossRef] [PubMed]
44. Umezawa, M.; Itano, R.; Sakaguchi, N.; Kawasaki, T. Infrared spectroscopy analysis determining secondary structure change in albumin by cerium oxide nanoparticles. *Front. Toxicol.* **2023**, *5*, 1237819. [CrossRef]
45. Kunc, F.; Gallerneault, M.; Kodra, O.; Brinkmann, A.; Lopinski, G.P.; Johnston, L.J. Surface chemistry of metal oxide nanoparticles: NMR and TGA quantification. *Anal. Bioanal. Chem.* **2022**, *414*, 4409–4425. [CrossRef]
46. Pop, O.L.; Mesaros, A.; Vodnar, D.C.; Suharoschi, R.; Tăbăran, F.; Mageruşan, L.; Tódor, I.S.; Diaconeasa, Z.; Balint, A.; Ciontea, L.; et al. Cerium Oxide Nanoparticles and Their Efficient Antibacterial Application In Vitro against Gram-Positive and Gram-Negative Pathogens. *Nanomaterials* **2020**, *10*, 1614. [CrossRef]
47. Zhou, L.; Li, X.; Yao, Z.; Chen, Z.; Hong, M.; Zhu, R.; Liang, Y.; Zhao, J. Transition-Metal Doped Ceria Microspheres with Nanoporous Structures for CO Oxidation. *Sci. Rep.* **2016**, *6*, 23900. [CrossRef] [PubMed]
48. Sakthiraj, K.; Karthikeyan, B. Synthesis and characterization of cerium oxide nanoparticles using different solvents for electrochemical applications. *Appl. Phys. A* **2019**, *126*, 52. [CrossRef]
49. Gopinath, K.; Karthika, V.; Sundaravadivelan, C.; Gowri, S.; Arumugam, A. Mycogenesis of cerium oxide nanoparticles using Aspergillus niger culture filtrate and their applications for antibacterial and larvicidal activities. *J. Nanostructure Chem.* **2015**, *5*, 295–303. [CrossRef]
50. Babitha, K.K.; Sreedevi, A.; Priyanka, K.P.; Sabu, B.; Varghese, T. Structural characterization and optical studies of CeO_2 nanoparticles synthesized by chemical precipitation. *Indian J. Pure Appl. Phys.* **2015**, *53*, 596–603.

51. Pansambal, S.; Oza, R.; Borgave, S.; Chauhan, A.; Bardapurkar, P.; Vyas, S.; Ghotekar, S. Bioengineered cerium oxide (CeO_2) nanoparticles and their diverse applications: A review. *Appl. Nanosci.* **2023**, *13*, 6067–6092. [CrossRef]
52. Wu, L.; Lei, X.; Zhang, Y.; Zhang, S.; Yang, G.; Zhang, P. The Tribological Mechanism of Cerium Oxide Nanoparticles as Lubricant Additive of Poly-Alpha Olefin. *Tribol. Lett.* **2020**, *68*, 101. [CrossRef]
53. Azman, N.F.; Samion, S. Dispersion Stability and Lubrication Mechanism of Nanolubricants: A Review. *Int. J. Precis. Eng. Manuf. Technol.* **2019**, *6*, 393–414. [CrossRef]
54. Ismail, M.F.; Azmi, W.H.; Mamat, R.; Sharma, K.V.; Zawawi, N.N. Stability Assessment of Polyvinyl-Ether-Based TiO_2, SiO_2, and Their Hybrid Nanolubricants. *Lubricants* **2023**, *11*, 23. [CrossRef]
55. Ismail, M.F.; Azmi, W.H.; Mamat, R.; Hamisa, A.H. Experimental Investigation on Newtonian Behaviour and Viscosity of TiO_2/PVE Nanolubricants for Application in Refrigeration System. *J. Adv. Res. Fluid Mech. Therm. Sci.* **2022**, *92*, 9–17. [CrossRef]
56. Hemmat Esfe, M.; Alidoust, S.; Toghraie, D. Study of rheological behavior of a hybrid nano-lubricant (MWCNT-Al_2O_3 (20:80)/SAE40) using two-way laboratory method and response surface methodology. *Arab. J. Chem.* **2023**, *16*, 104530. [CrossRef]
57. Nyholm, N.; Espallargas, N. Functionalized carbon nanostructures as lubricant additives—A review. *Carbon N. Y.* **2023**, *201*, 1200–1228. [CrossRef]
58. Al-Janabi, A.S.; Hussin, M.; Htwe, Y.Z.N.; Yasmin, W. Experimental investigation on the tribological and rheological properties of graphene and FMWCNT based nanolubricants with CTAB surfactants. *Synth. Met.* **2024**, *308*, 117726. [CrossRef]
59. Ghannam, M.T.; Selim, M.Y.E.; Khedr, M.A.M.; Bin Taleb, N.A.G.; Kaalan, N.R. Investigation of the rheological properties of waste and pure lube oils. *Fuel* **2021**, *298*, 120774. [CrossRef]
60. Álvarez-Asencio, R.; Corkery, R.W.; Ahniyaz, A. Solventless synthesis of cerium oxide nanoparticles and their application in UV protective clear coatings. *RSC Adv.* **2020**, *10*, 14818–14825. [CrossRef]
61. Kotia, A.; Rajkhowa, P.; Rao, G.S.; Ghosh, S.K. Thermophysical and tribological properties of nanolubricants: A review. *Heat Mass Transf.* **2018**, *54*, 3493–3508. [CrossRef]
62. Kedzierski, M.A. Viscosity and density of aluminum oxide nanolubricant. *Int. J. Refrig.* **2013**, *36*, 1333–1340. [CrossRef]
63. Sharif, M.Z.; Azmi, W.H.; Ghazali, M.F.; Zawawi, N.N.M.; Ali, H.M. Viscosity and Friction Reduction of Double-End-Capped Polyalkylene Glycol Nanolubricants for Eco-Friendly Refrigerant. *Lubricants* **2023**, *11*, 129. [CrossRef]
64. Ahmed Ali, M.K.; Xianjun, H.; Abdelkareem, M.A.A.; Elsheikh, A.H. Role of Nanolubricants Formulated in Improving Vehicle Engines Performance. *IOP Conf. Ser. Mater. Sci. Eng.* **2019**, *563*, 022015. [CrossRef]
65. Dale, J.G.; Cox, S.S.; Vance, M.E.; Marr, L.C.; Hochella, M.F. Transformation of Cerium Oxide Nanoparticles from a Diesel Fuel Additive during Combustion in a Diesel Engine. *Environ. Sci. Technol.* **2017**, *51*, 1973–1980. [CrossRef]
66. Marquis, F.D.S.; Chibante, L.P.F. Improving the heat transfer of nanofluids and nanolubricants with carbon nanotubes. *JOM* **2005**, *57*, 32–43. [CrossRef]
67. Uflyand, I.E.; Zhinzhilo, V.A.; Burlakova, V.E. Metal-containing nanomaterials as lubricant additives: State-of-the-art and future development. *Friction* **2019**, *7*, 93–116. [CrossRef]
68. Rao, T.S.; Babu Rao, H.S.; Jilani, S.A.K.; Mutluri, A. Effect of Cerium Oxide Nanoparticles Additive Blended in Palm Oil Biodiesel as Alternative Fuel Used in Diesel Engine. *IOP Conf. Ser. Mater. Sci. Eng.* **2021**, *1112*, 12012. [CrossRef]
69. Zhao, J.; Huang, Y.; He, Y.; Shi, Y. Nanolubricant additives: A review. *Friction* **2021**, *9*, 891–917. [CrossRef]
70. Zhang, F.; Chan, S.-W.; Spanier, J.E.; Apak, E.; Jin, Q.; Robinson, R.D.; Herman, I.P. Cerium oxide nanoparticles: Size-selective formation and structure analysis. *Appl. Phys. Lett.* **2002**, *80*, 127–129. [CrossRef]
71. Liu, X.; He, X.; Zhang, J.; Yang, J.; Xiang, X.; Ma, Z.; Liu, L.; Zong, E. Cerium oxide nanoparticle functionalized lignin as a nano-biosorbent for efficient phosphate removal. *RSC Adv.* **2020**, *10*, 1249–1260. [CrossRef]
72. Archard, J.F. Contact and rubbing of flat surfaces. *J. Appl. Phys.* **1953**, *24*, 981–988. [CrossRef]
73. Kuang, X.; Yin, B.; Wang, J.; Jia, H.; Xu, B. Dispersion stability and wear properties of nano-CeO as lubricating oil additives for engines. *Ind. Lubr. Tribol.* **2022**, *74*, 813–819. [CrossRef]
74. de Oliveira, L.R.; Rodrigues, T.A.; Costa, H.L.; da Silva, W.M., Jr. Scuffing resistance of polyalphaolefin (PAO)-based nanolubricants with oleic acid (OA) and iron oxide nanoparticles. *Mater. Today Commun.* **2022**, *31*, 103837. [CrossRef]